22 Pos W, Crawley JT, Fijnheer R, Voorberg J, Lane DA, Luken BM. An autoantibody epitope comprising residues R660, Y661, and Y665 in the ADAMTS13 spacer domain identifies a binding site for the A2 domain of VWF. *Blood* 2010; **115**: 1640–9.
23 Akiyama M, Takeda S, Kokame K, Takagi J, Miyata T. Production, crystallization and preliminary crystallographic analysis of an exosite-containing fragment of human von Willebrand factor-cleaving proteinase ADAMTS13. *Acta Crystallogr F Struct Biol Crystallogr Commun* 2009; **65**: 739–42.
24 Reeves PJ, Callewaert N, Contreras R, Khorana HG. Structure and function in rhodopsin: high-level expression of rhodopsin with restricted and homogeneous *N*-glycosylation by a tetracycline-inducible *N*-acetylglucosaminyltransferase I-negative HEK293S stable mammalian cell line. *Proc Natl Acad Sci USA* 2002; **99**: 13419–24.
25 Winn MD, Ballard CC, Cowtan KD, Dodson EJ, Emsley P, Evans PR, Keegan RM, Krissinel EB, Leslie AG, McCoy A, McNicholas SJ, Murshudov GN, Pannu NS, Potterton EA, Powell HR, Read RJ, Vagin A, Wilson KS. Overview of the CCP4 suite and current developments. *Acta Crystallogr D Biol Crystallogr* 2011; **67**: 235–42.
26 Emsley P, Lohkamp B, Scott WG, Cowtan K. Features and development of Coot. *Acta Crystallogr D Biol Crystallogr* 2010; **66**: 486–501.
27 Brunger AT. Version 1.2 of the crystallography and NMR system. *Nat Protoc* 2007; **2**: 2728–33.
28 Kokame K, Nobe Y, Kokubo Y, Okayama A, Miyata T. FRETS-VWF73, a first fluorogenic substrate for ADAMTS13 assay. *Br J Haematol* 2005; **129**: 93–100.
29 Anderson PJ, Kokame K, Sadler JE. Zinc and calcium ions cooperatively modulate ADAMTS13 activity. *J Biol Chem* 2006; **281**: 850–7.
30 Zhang P, Pan W, Rux AH, Sachais BS, Zheng XL. The cooperative activity between the carboxyl-terminal TSP1 repeats and the CUB domains of ADAMTS13 is crucial for recognition of von Willebrand factor under flow. *Blood* 2007; **110**: 1887–94.
31 De Marco L, Shapiro SS. Properties of human asialo-factor VIII. A ristocetin-independent platelet-aggregating agent. *J Clin Invest* 1981; **68**: 321–8.
32 Gonzalez de Peredo A, Klein D, Macek B, Hess D, Peter-Katalinic J, Hofsteenge J. *C*-mannosylation and *O*-fucosylation of thrombospondin type 1 repeats. *Mol Cell Proteomics* 2002; **1**: 11–18.
33 Wang LW, Leonhard-Melief C, Haltiwanger RS, Apte SS. Post-translational modification of thrombospondin type-1 repeats in ADAMTS-like 1/punctin-1 by *C*-mannosylation of tryptophan. *J Biol Chem* 2009; **284**: 30004–15.
34 Zhang Q, Zhou YF, Zhang CZ, Zhang X, Lu C, Springer TA. Structural specializations of A2, a force-sensing domain in the ultralarge vascular protein von Willebrand factor. *Proc Natl Acad Sci USA* 2009; **106**: 9226–31.
35 Zhang X, Halvorsen K, Zhang CZ, Wong WP, Springer TA. Mechanoenzymatic cleavage of the ultralarge vascular protein von Willebrand factor. *Science* 2009; **324**: 1330–4.
36 Zakai NA, McClure LA. Racial differences in venous thromboembolism. *J Thromb Haemost* 2011; **9**: 1877–82.
37 Miyata T, Hamasaki N, Wada H, Kojima T. More on: racial differences in venous thromboembolism. *J Thromb Haemost* 2012; **10**: 319–20.
38 Zhou W, Bouhassira EE, Tsai HM. An IAP retrotransposon in the mouse ADAMTS13 gene creates ADAMTS13 variant proteins that are less effective in cleaving von Willebrand factor multimers. *Blood* 2007; **110**: 886–93.
39 Kokame K, Matsumoto M, Fujimura Y, Miyata T. VWF73, a region from D1596 to R1668 of von Willebrand factor, provides a minimal substrate for ADAMTS-13. *Blood* 2004; **103**: 607–12.

Table S1. Data collection and refinement statistics.

	ADAMTS13-DTCS-P475S
PDB ID	3VN4
Data collection	
Space group	*C2*
Cell dimensions	
a, *b*, *c* (Å)	153.4, 53.2, 76.6
α, β, γ (°)	90.0, 111.6, 90.0
Wavelength (Å)	1.0
Resolution (Å)	50.0–2.8 (2.9–2.8)
No. of unique reflections	14278 (1405)
R_{merge}	0.048 (0.310)
I / s(I)	36.1 (6.3)
Completeness (%)	99.1 (99.0)
Redundancy	3.7 (3.7)
No. of protein molecules in ASU	1
Refinement	
Resolution (Å)	30.9-2.8 (2.87–2.80)
No. reflections	13509 (929)
R_{work}	0.229 (0.283)
R_{free}	0.275 (0.354)
No. atoms	
Protein	2895
Carbohydrate	74
Water	45
B-factors	
Protein	72.2
Carbohydrate	66.4
Water	62.9
R.m.s deviations	
Bond lengths (Å)	0.006
Bond angles (°)	0.95
*Ramachandran	
Favored (%)	96.21
Outlier (%)	1
*MolProbity score	1.71 (100^{th} percentile)
*Clash score	5.52 (100^{th} percentile)

Single crystals were used for each data set. Values in parentheses are for the highest-resolution shell. *The accuracy of the model was judged by the MolProbity server (http://molprobity.biochem.duke.edu/).

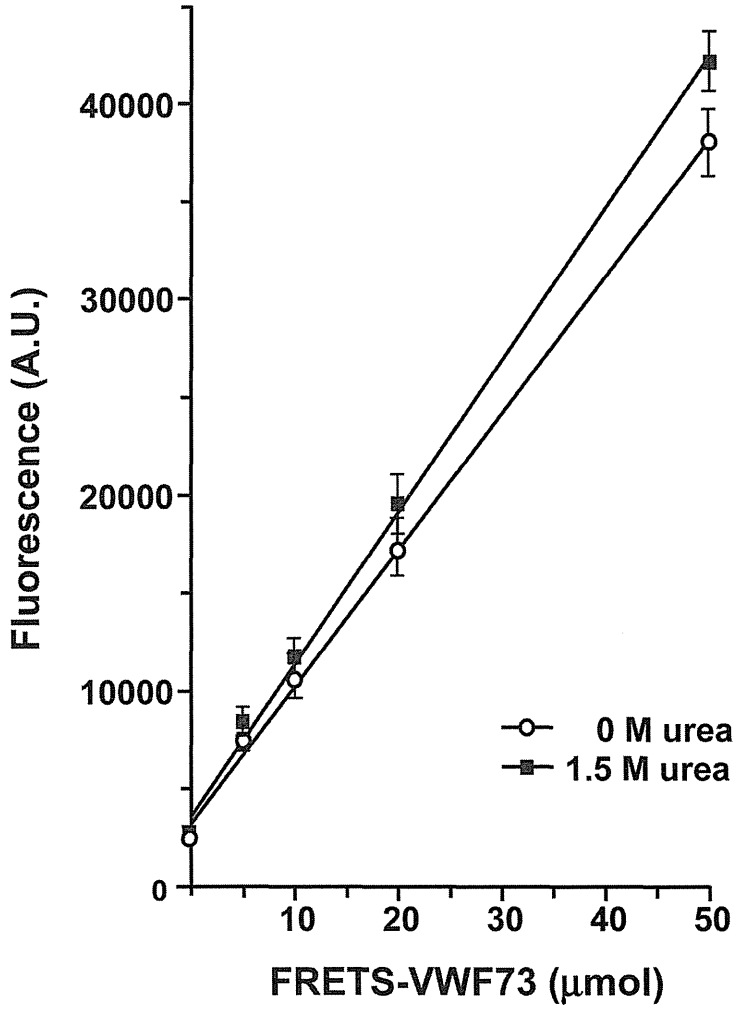
Fluorescence (A.U.)
40000
30000
20000
10000
0
10
20
30
40
50
FRETS-VWF73 (µmol)
0 M urea
1.5 M urea

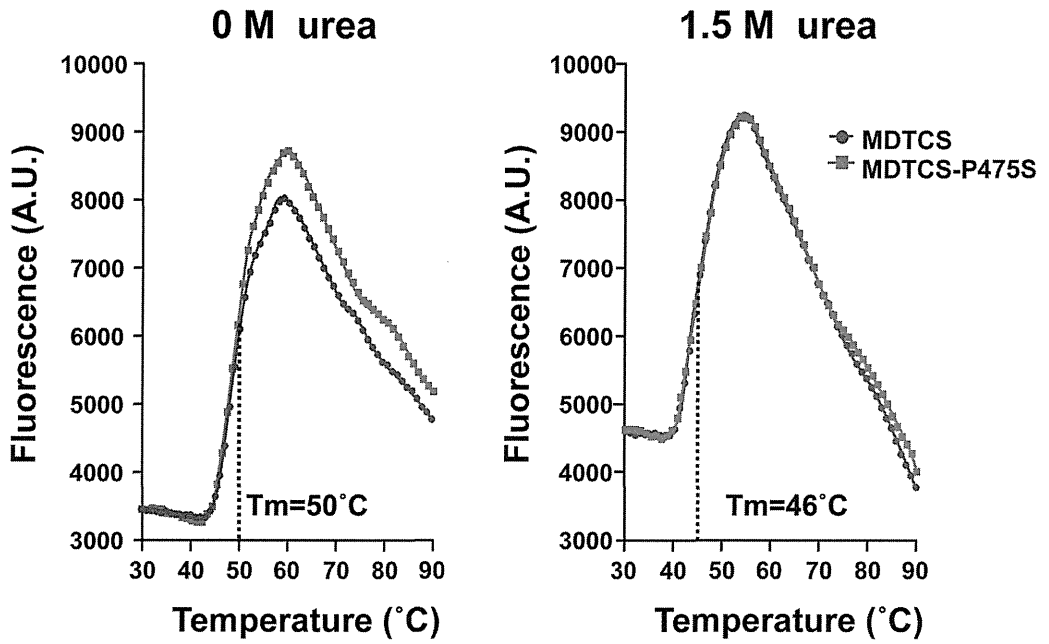
0 M urea
1.5 M urea
Fluorescence (A.U.)
Temperature (˚C)
Tm=50˚C
Tm=46˚C
MDTCS
MDTCS-P475S
10000
9000
8000
7000
6000
5000
4000
3000
30 40 50 60 70 80 90

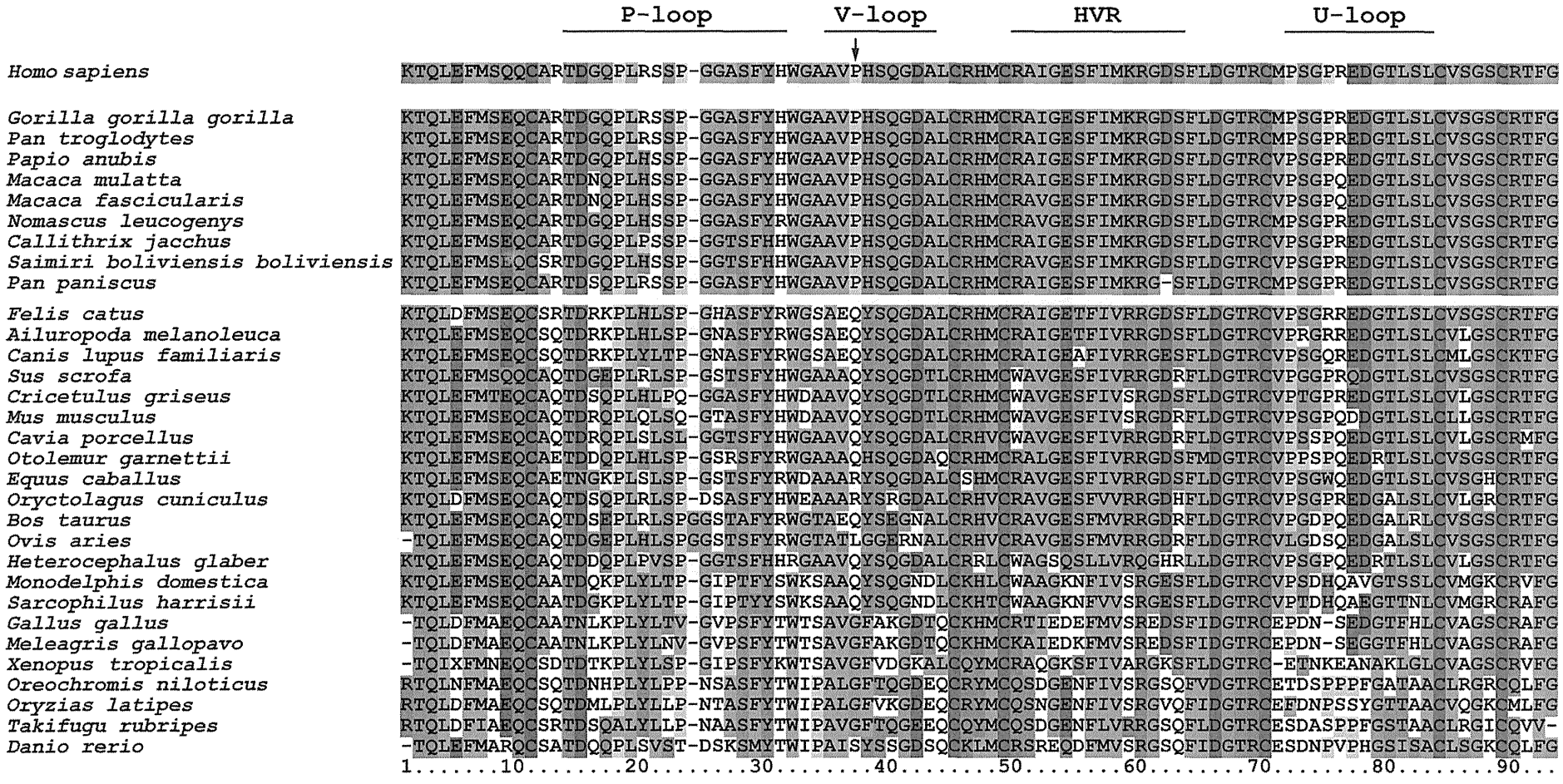
P-loop
V-loop
HVR
U-loop
Homo sapiens KTQLEFMSQQCARTDGQPLRSSP-GGASFYHWGAAVPHSQGDALCRHMCRAIGESFIMKRGDSFLDGTRCMPSGPREDGTLSLCVSGSCRTFG
Gorilla gorilla gorilla KTQLEFMSEQCARTDGQPLRSSP-GGASFYHWGAAVPHSQGDALCRHMCRAIGESFIMKRGDSFLDGTRCMPSGPREDGTLSLCVSGSCRTFG
Pan troglodytes KTQLEFMSEQCARTDGQPLRSSP-GGASFYHWGAAVPHSQGDALCRHMCRAIGESFIMKRGDSFLDGTRCMPSGPREDGTLSLCVSGSCRTFG
Papio anubis KTQLEFMSEQCARTDGQPLHSSP-GGASFYHWGAAVPHSQGDALCRHMCRAIGESFIMKRGDSFLDGTRCVPSGPREDGTLSLCVSGSCRTFG
Macaca mulatta KTQLEFMSEQCARTDNQPLHSSP-GGASFYHWGAAVPHSQGDALCRHMCRAIGESFIMKRGDSFLDGTRCVPSGPQEDGTLSLCVSGSCRTFG
Macaca fascicularis KTQLEFMSEQCARTDNQPLHSSP-GGASFYHWGAAVPHSQGDALCRHMCRAVGESFIMKRGDSFLDGTRCVPSGPQEDGTLSLCVSGSCRTFG
Nomascus leucogenys KTQLEFMSEQCARTDGQPLHSSP-GGASFYRWGAAVPHSQGDALCRHMCRAVGESFIMKRGDSFLDGTRCMPSGPREDGTLSLCVSGSCRTFG
Callithrix jacchus KTQLEFMSEQCARTDGQPLPSSP-GGTSFHHWGAAVPHSQGDALCRHMCRAIGESFIMKRGDSFLDGTRCVPSGPREDGTLSLCVSGSCRTFG
Saimiri boliviensis boliviensis KTQLEFMSLQCSRTDGQPLHSSP-GGTSFHHWGAAVPHSQGDALCRHMCRAVGESFIMKRGDSFLDGTRCVPSGPREDGTLSLCVSGSCRTFG
Pan paniscus KTQLEFMSEQCARTDSQPLRSSP-GGASFYHWGAAVPHSQGDALCRHMCRAIGESFIMKRG-SFLDGTRCMPSGPREDGTLSLCVSGSCRTFG
Felis catus KTQLDFMSEQCSRTDRKPLHLSP-GHASFYRWGSAEQYSQGDALCRHMCRAIGETFIVRRGDSFLDGTRCVPSGRREDGTLSLCVSGSCRTFG
Ailuropoda melanoleuca KTQLEFMSEQCSQTDRKPLHLSP-GNASFYRWGSAEQYSQGDALCRHMCRAIGETFIVRRGDSFLDGTRCVPRGRREDGTLSLCVLGSCRTFG
Canis lupus familiaris KTQLEFMSEQCSQTDRKPLYLTP-GNASFYRWGSAEQYSQGDALCRHMCRAIGEAFIVRRGESFLDGTRCVPSGQREDGTLSLCMLGSCKTFG
Sus scrofa KTQLEFMSQQCAQTDGEPLRLSP-GSTSFYHWGAAAQYSQGDTLCRHMCWAVGESFIVRRGDRFLDGTRCVPGGPRQDGTLSLCVSGSCRTFG
Cricetulus griseus KTQLEFMTEQCAQTDSQPLHLPQ-GGASFYHWDAAVQYSQGDTLCRHMCWAVGESFIVSRGDSFLDGTRCVPTGPREDGTLSLCVLGSCRTFG
Mus musculus KTQLEFMSEQCAQTDRQPLQLSQ-GTASFYHWDAAVQYSQGDTLCRHMCWAVGESFIVSRGDRFLDGTRCVPSGPQDDGTLSLCLLGSCRTFG
Cavia porcellus KTQLEFMSEQCAQTDRQPLSLSL-GGTSFYHWGAAVQYSQGDALCRHVCWAVGESFIVRRGDRFLDGTRCVPSSPQEDGTLSLCVLGSCRMFG
Otolemur garnettii KTQLEFMSEQCAETDDQPLHLSP-GSRSFYRWGAAAQHSQGDAQCRHMCRALGESFIVRRGDSFMDGTRCVPPSPQEDRTLSLCVSGSCRTFG
Equus caballus KTQLEFMSEQCAETNGKPLSLSP-GSTSFYRWDAAARYSQGDALCSHMCRAVGESFIVRRGDSFLDGTRCVPSGWQEDGTLSLCVSGHCRTFG
Oryctolagus cuniculus KTQLDFMSEQCAQTDSQPLRLSP-DSASFYHWEAAARYSRGDALCRHVCRAVGESFVVRRGDHFLDGTRCVPSGPREDGALSLCVLGRCRTFG
Bos taurus KTQLEFMSEQCAQTDSEPLRLSPGGSTAFYRWGTAEQYSEGNALCRHVCRAVGESFMVRRGDRFLDGTRCVPGDPQEDGALRLCVSGSCRTFG
Ovis aries -TQLEFMSEQCAQTDGEPLHLSPGGSTSFYRWGTATLGGERNALCRHVCRAVGESFMVRRGDRFLDGTRCVLGDSQEDGALSLCVSGSCRTFG
Heterocephalus glaber KTQLEFMSEQCAQTDDQPLPVSP-GGTSFHHRGAAVQYSQGDALCRRLCWAGSQSLLVRQGHRLLDGTRCVPSGPQEDRTLSLCVLGSCRTFG
Monodelphis domestica KTQLEFMSEQCAATDQKPLYLTP-GIPTFYSWKSAAQYSQGNDLCKHLCWAAGKNFIVSRGESFLDGTRCVPSDHQAVGTSSLCVMGKCRVFG
Sarcophilus harrisii KTQLEFMSEQCAATDGKPLYLTP-GIPTYYSWKSAAQYSQGNDLCKHTCWAAGKNFVVSRGESFLDGTRCVPTDHQAEGTTNLCVMGRCRAFG
Gallus gallus -TQLDFMAEQCAATNLKPLYLTV-GVPSFYTWTSAVGFAKGDTQCKHMCRTIEDEFMVSREDSFIDGTRCEPDN-SEDGTFHLCVAGSCRAFG
Meleagris gallopavo -TQLDFMAEQCAATNLKPLYLNV-GVPSFYTWTSAVGFAKGDTQCKHMCKAIEDKFMVSREDSFIDGTRCEPDN-SEGGTFHLCVAGSCRAFG
Xenopus tropicalis -TQIXFMNEQCSDTDTKPLYLSP-GIPSFYKWTSAVGFVDGKALCQYMCRAQGKSFIVARGKSFLDGTRC-ETNKEANAKLGLCVAGSCRVFG
Oreochromis niloticus RTQLNFMAEQCSQTDNHPLYLPP-NSASFYTWIPALGFTQGDEQCRYMCQSDGENFIVSRGSQFVDGTRCETDSPPPFGATAACLRGRCQLFG
Oryzias latipes RTQLDFMAEQCSQTDMLPLYLLP-NTASFYTWIPALGFVKGDEQCRYMCQSNGENFIVSRGVQFIDGTRCEFDNPSSYGTTAACVQGKCMLFG
Takifugu rubripes RTQLDFIAEQCSRTDSQALYLLP-NAASFYTWIPAVGFTQGEEQCQYMCQSDGENFLVRRGSQFLDGTRCESDASPPFGSTAACLRGICQVV-
Danio rerio -TQLEFMARQCSATDQQPLSVST-DSKSMYTWIPAISYSSGDSQCKLMCRSREQDFMVSRGSQFIDGTRCESDNPVPHGSISACLSGKCQLFG
1.....10.....20.....30.....40.....50.....60.....70.....80.....90...

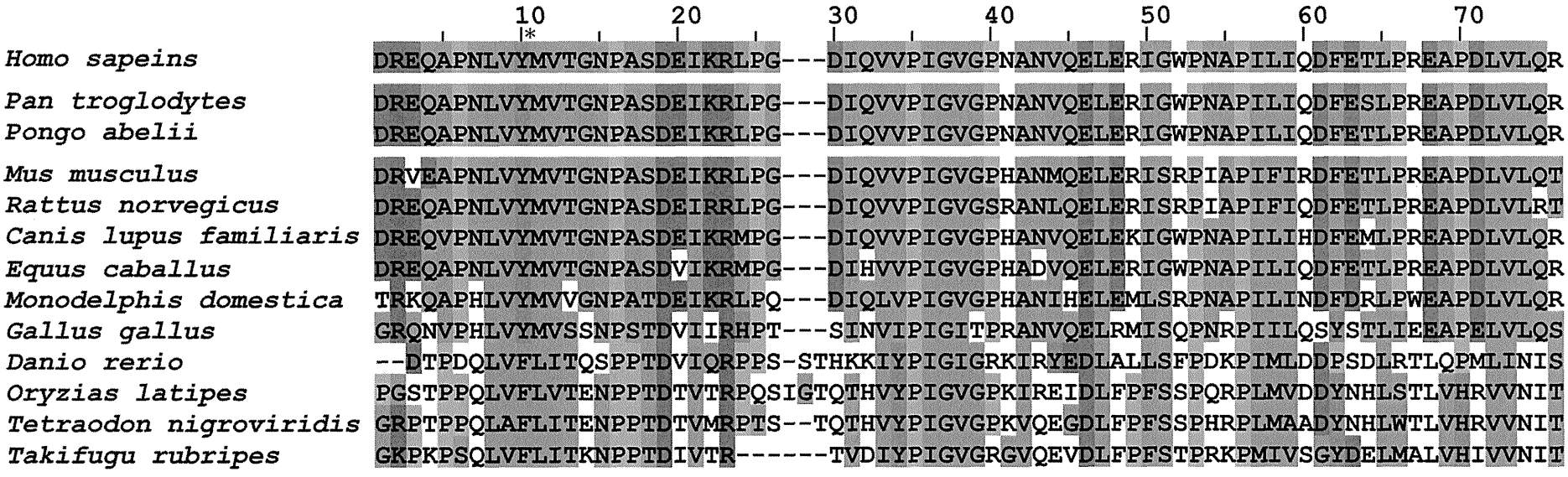
10
20
30
40
50
60
70
*
Homo sapeins DREQAPNLVYMVTGNPASDEIKRLPG---DIQVVPIGVGPNANVQELERIGWPNAPILIQDFETLPREAPDLVLQR
Pan troglodytes DREQAPNLVYMVTGNPASDEIKRLPG---DIQVVPIGVGPNANVQELERIGWPNAPILIQDFESLPREAPDLVLQR
Pongo abelii DREQAPNLVYMVTGNPASDEIKRLPG---DIQVVPIGVGPNANVQELERIGWPNAPILIQDFETLPREAPDLVLQR
Mus musculus DRVEAPNLVYMVTGNPASDEIKRLPG---DIQVVPIGVGPHANMQELERISRPIAPIFIRDFETLPREAPDLVLQT
Rattus norvegicus DREQAPNLVYMVTGNPASDEIRRLPG---DIQVVPIGVGSRANLQELERISRPIAPIFIQDFETLPREAPDLVLRT
Canis lupus familiaris DREQVPNLVYMVTGNPASDEIKRMPG---DIQVVPIGVGPHANVQELEKIGWPNAPILIHDFEMLPREAPDLVLQR
Equus caballus DREQAPNLVYMVTGNPASDVIKRMPG---DIHVVPIGVGPHADVQELERIGWPNAPILIQDFETLPREAPDLVLQR
Monodelphis domestica TRKQAPHLVYMVVGNPATDEIKRLPQ---DIQLVPIGVGPHANIHELEMLSRPNAPILINDFDRLPWEAPDLVLQR
Gallus gallus GRQNVPHLVYMVSSNPSTDVIIRHPT---SINVIPIGITPRANVQELRMISQPNRPIILQSYSTLIEEAPELVLQS
Danio rerio --DTPDQLVFLITQSPPTDVIQRPPS-STHKKIYPIGIGRKIRYEDLALLSFPDKPIMLDDPSDLRTLQPMLINIS
Oryzias latipes PGSTPPQLVFLVTENPPTDTVTRPQSIGTQTHVYPIGVGPKIREIDLFPFSSPQRPLMVDDYNHLSTLVHRVVNIT
Tetraodon nigroviridis GRPTPPQLAFLITENPPTDTVMRPTS--TQTHVYPIGVGPKVQEGDLFPFSSPHRPLMAADYNHLWTLVHRVVNIT
Takifugu rubripes GKPKPSQLVFLITKNPPTDIVTR------TVDIYPIGVGRGVQEVDLFPFSTPRKPMIVSGYDELMALVHIVVNIT

British Journal of Nutrition (2013), **110**, 2150–2155
doi:10.1017/S0007114513001670

Up-regulation of endothelial nitric oxide synthase (*eNOS*), silent mating type information regulation 2 homologue 1 (*SIRT1*) and autophagy-related genes by repeated treatments with resveratrol in human umbilical vein endothelial cells

Yoshie Takizawa[1]†, Yukiko Kosuge[1]†, Hiroyo Awaji[1], Emi Tamura[1], Ayako Takai[1], Takaaki Yanai[2], Reiko Yamamoto[2], Koichi Kokame[3], Toshiyuki Miyata[3], Rieko Nakata[1] and Hiroyasu Inoue[1]*

[1]*Department of Food Science and Nutrition, Nara Women's University, Kita-Uoya-Nishi-Machi, Nara 630-8506, Japan*
[2]*Mercian Corporation, Product Development Research Laboratory, Fujisawa 251-0057, Japan*
[3]*Department of Molecular Pathogenesis, National Cerebral and Cardiovascular Center, Osaka 565-8565, Japan*

(Submitted 4 January 2013 – Final revision received 27 March 2013 – Accepted 29 April 2013 – First published online 11 June 2013)

Abstract

Resveratrol, a polyphenolic phytoalexin found in red wine and various plants, has been reported to up-regulate the expression of endothelial NO synthase (eNOS) in human umbilical vein endothelial cells (HUVEC). However, this effect was neither long term in nature nor physiologically relevant at the concentration of resveratrol studied. In the present study, we investigated the effects of repeated treatments with a lower concentration of resveratrol on the expression of genes in HUVEC. The expression levels of eNOS and silent mating type information regulation 2 homologue 1 (SIRT1) were up-regulated in HUVEC by repeated treatments with 1 μM-resveratrol for 6 d, but not with fenofibrate. Moreover, resveratrol treatment increased the expression of autophagy-regulated genes such as γ-aminobutyric acid A receptor-associated protein (*GABARAP*), microtubule-associated protein 1 light chain 3B (*LC3B*) and autophagy-related protein 3 (*ATG3*), the radical scavenger activity-related metallothionein-1X (*MT1X*) gene and the anti-inflammatory activity-related annexin A2 (*ANXA*) gene. In addition, resveratrol treatment down-regulated the expression of the cell-cycle checkpoint control RAD9 homologue B (*RAD9B*) gene. These results indicate the beneficial effects of resveratrol on the cardiovascular system.

Key words: Resveratrol: Endothelial nitric oxide synthase: Silent mating type information regulation 2 homologue 1: Autophagy

The prevention of lifestyle-related diseases such as CVD, diabetes and stroke has attracted worldwide interest. Current treatment regimens for lifestyle-related diseases have shifted their focus onto the functionality of natural chemicals present in foods and drinks. One example is the association between the long-term consumption of red wine and reduced risk for CVD. In this context, resveratrol, a phytoalexin and antioxidant polyphenol present in red wine and various plants, has emerged as one of the most attractive and extensively studied compounds[1,2].

We have previously demonstrated that resveratrol suppresses the expression of cyclo-oxygenase (COX)-2, the rate-limiting enzyme in PG biosynthesis[3], particularly in 184B5/HER(184B5/human EGFR-related-2)-transformed mammary epithelial cells[4]. Additionally, we have shown that resveratrol activates PPARα, PPARβδ and PPARγ[5,6], which are members of the nuclear receptor family of ligand-dependent transcription factors[7,8]; that it protects the brain against ischaemic stroke in mice through a PPARα-dependent mechanism demonstrated in cell-based reporter assays[5] and that it acts via a negative feedback loop mediated through PPARγ to inhibit the expression of COX-2, particularly in macrophages[9]. Based on these data, we have focused our attention on PPAR as potential molecular targets of resveratrol in the prevention of lifestyle-related diseases, the molecular mechanisms of which remain to be determined.

Previous studies have investigated the effects of resveratrol on the activation of silent mating type information regulation 2 homologue 1 (SIRT1), a NAD^+-dependent protein

Abbreviations: BAEC, bovine arterial endothelial cells; COX, cyclo-oxygenase; eNOS, endothelial nitric oxide synthase; HUVEC, human umbilical vein endothelial cells; RAD9B, RAD9 homologue B; SIRT1, silent mating type information regulation 2 homologue 1.

***Corresponding author:** Dr H. Inoue, fax +81 742 20 3458, email inoue@cc.nara-wu.ac.jp

† Both authors contributed equally to this work.

British Journal of Nutrition

deacetylase[10–12], although a direct activation was not observed[13,14]. Resveratrol has been reported to enhance the expression of endothelial NO synthase (eNOS)[15], which may be important for elucidating the effects of resveratrol on the cardiovascular system. However, these observations were based on human umbilical vein endothelial cells (HUVEC) treated with 33 μM-resveratrol for 24 h, conditions which are neither long term in nature nor physiologically relevant, and a time (24–72 h)- and concentration-dependent up-regulation of the expression of eNOS (2·8-fold in 100 μM-resveratrol) was observed not in HUVEC but in the EA.hy926 cell line, which is a hybrid of the HUVEC and human lung carcinoma A549 cells[15].

In the present study, we investigated the effects of resveratrol on the expression of eNOS using a physiological concentration (1 μM) during repeated treatments for 6 d. We demonstrated that the expression of eNOS and SIRT1 is up-regulated by resveratrol. We screened the differentially regulated genes in HUVEC on resveratrol treatment using microarray analysis and confirmed the candidate genes using quantitative RT-PCR analysis. We demonstrated that resveratrol increases the expression of autophagy-related genes, γ-aminobutyric acid A receptor-associated protein (*GABARAP*), microtubule-associated protein 1 light chain 3B (*LC3B*) and autophagy-related protein 3 (*ATG3*), and the radical scavenger activity-related metallothionein-1X (*MT1X*) gene. Additionally, we demonstrated that the expression of the cell-cycle checkpoint control RAD9 homologue B (*RAD9B*) gene is down-regulated by resveratrol. These data help in the identification of molecular mechanisms that may contribute to the beneficial effects of resveratrol on the cardiovascular system.

Experimental methods

Cell culture

HUVEC were obtained from the Japanese Collection of Research Bioresources and were grown in an endothelial cell growth medium (Cell Applications, Inc.). The cells were cultured for 6 d in the presence or absence of 1 μM-resveratrol or 1 μM-fenofibrate, a synthetic PPARα agonist, with the media being changed at 0, 2 and 4 d.

RNA extraction and analysis

Total RNA was isolated from the HUVEC using the acid guanidinium thiocyanate procedure and was analysed for gene expression via real-time quantitative RT-PCR (Mx3005; Stratagene) as described previously[16]. The primer pairs for the genes used in the present study and the cycling conditions are given in Table S1 (available online). The expression level of each mRNA was normalised to that of the glyceraldehyde-3-phosphate dehydrogenase (*GAPDH*) mRNA, which has been used for our previous study in HUVEC[5,17]and bovine arterial endothelial cells (BAEC)[9,16].

DNA microarray analysis

HUVEC were cultured for 6 d in the presence or absence of 1 μM-resveratrol. DNA microarray analysis was performed as described previously[18]. Briefly, poly(A)$^+$ RNA was prepared from resveratrol-treated and untreated HUVEC using a QuickPrep micro mRNA purification kit (GE Healthcare) and was used to prepare complementary RNA samples as described in the GeneChip Expression Analysis Technical Manual (Affymetrix). Double-stranded complementary DNA was synthesised from 0·6 μg of poly(A)$^+$ RNA using a Message-AMP™ II aRNA amplification kit (PE Applied Biosystems) with T7-$(dT)_{24}$ primer (GE Healthcare). The product served as a template for the synthesis of biotin-labelled complementary RNA via *in vitro* transcription using a GeneChip IVT labelling kit (Affymetrix), and the amplified complementary RNA was fragmented by heat treatment in the presence of potassium acetate and magnesium acetate. The complementary RNA sample (10 μg) was then applied to a GeneChip Human Genome U133 Plus 2.0 Array (Affymetrix), and hybridisation, washing, staining and scanning were performed according to the GeneChip Manual. The data for each probe set were calculated from the scanned array image using the GeneChip Analysis Suite (Affymetrix) and GeneSpring (Agilent Technologies). The procedure of analysis was as follows: for background subtraction, the median value of the negative control genes was subtracted from the raw values for each gene, and the resulting values were divided by the value of the 50th percentile of each chip to normalise the various signal intensities among the arrays. Finally, the ratios (resveratrol-treated:untreated and untreated:resveratrol-treated) were calculated from the average of duplicate normalised signal intensities. A change in expression of 1·5-fold was used as a threshold for comparison.

Statistical analysis

All results are expressed as the means and standard deviations. Comparisons between the groups were made using one-way ANOVA with *post hoc* Bonferroni multiple-comparison test or the unpaired *t* test. A P value $<0·05$ was considered to indicate statistical significance.

Results and discussion

Repeated treatments with resveratrol up-regulate the expression of endothelial nitric oxide synthase

HUVEC were cultured for 6 d in the presence or absence of 1 μM-resveratrol and examined for the expression of eNOS by quantitative RT-PCR (Fig. 1(a)). The levels of *eNOS* mRNA were up-regulated 1·5-fold. Previous studies have demonstrated approximately 1·4-fold up-regulation of *eNOS* mRNA levels in HUVEC following treatment with 33 μM-resveratrol, but not with 1 μM, for 24 h[15], indicating that long-term repeated treatments with 1 μM-resveratrol for 6 d, as done in the present study, lead to the up-regulation of *eNOS* mRNA levels. Our results are in agreement with the report that daily treatment with resveratrol significantly increases the production of both eNOS protein and NO in HUVEC[19]. Thus, induction of the expression of eNOS by repeated treatments with a physiological concentration of

British Journal of Nutrition

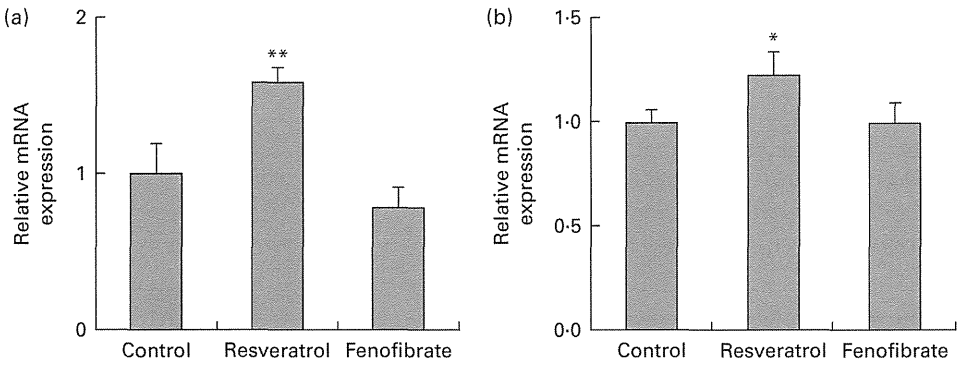

Fig. 1. Up-regulation of the expression of endothelial nitric oxide synthase (*eNOS*) and silent mating type information regulation 2 homologue 1 (*SIRT1*) mRNA and protein in human umbilical vein endothelial cells (HUVEC) following repeated treatments with 1 μM-resveratrol for 6 d. HUVEC were cultured for 6 d in the presence or absence of 1 μM-resveratrol or 1 μM-fenofibrate. Isolated RNA from the HUVEC was used for quantitative RT-PCR analysis. The mRNA levels of (a) *eNOS* and (b) *SIRT1* were normalised to that of the glyceraldehyde-3-phosphate dehydrogenase (*GAPDH*) mRNA. The normalised levels of *eNOS* and *SIRT1* mRNA in the absence of resveratrol are expressed as 1, respectively. Values are means of three separate dishes, with standard deviations represented by vertical bars. Mean values were significantly different from those of the control and fenofibrate treatments: * $P<0{\cdot}05$ and ** $P<0{\cdot}01$ (one-way ANOVA with *post hoc* Bonferroni multiple-comparison test). Similar results were obtained by two additional experiments.

resveratrol can account, in part, for the cardiovascular benefits of the long-term consumption of red wine.

Repeated treatments with resveratrol up-regulate the expression of silent mating type information regulation 2 homologue 1

We examined the expression levels of *SIRT1* mRNA (Fig. 1(b)) in HUVEC treated with 1 μM-resveratrol for 6 d. The levels of *SIRT1* mRNA were up-regulated by 1·2-fold. As previous studies have reported that resveratrol is not a direct activator of SIRT1[13,14], we sought to investigate the mechanism of the up-regulation of SIRT1 levels. We have previously demonstrated that resveratrol is a triple agonist for PPARα, PPARβ/δ and PPARγ *in vitro* [5,6] and that 4-week intake of resveratrol as well as the synthetic PPARα agonist fenofibrate up-regulates the hepatic expression of SIRT1 in wild-type, but not in *PPARα* knockout, mice (R Nakata *et al.*, unpublished results). Therefore, we examined the expression of SIRT1 in HUVEC treated with 1 μM-fenofibrate for 6 d and observed that *SIRT1* mRNA levels were unregulated by fenofibrate (Fig. 1(b)). Similarly, no effect on the expression of eNOS was observed following fenofibrate treatment (Fig. 1(a)). These discrepancies between the present study using HUVEC *in vitro* and the *PPARα* knockout mice study *in vivo* indicate the limitations of the present study. Cell culture of HUVEC is more difficult than that of BAEC since the former need several special supplements such as epidermal growth factor, basic fibroblast growth factor and vascular endothelial growth factor. Moreover, there are no interactions between HUVEC and other types of cells, which is common *in vivo*. On the other hand, fasting is reported to promote the expression of SIRT1 via the activation of PPARα in mice[20], whereas there is no report of a connection between the up-regulation of eNOS levels and the activation of PPARα. Therefore, we could

Table 1. Representative genes differentially expressed following repeated treatments with resveratrol

Gene	Fold change	GenBank no.
Up-regulated		
Human DNA sequence from clone RP4-581F12 on chromosome Xq21	× 3·6	AL031313
γ-Aminobutyric acid A receptor-associated protein (*GABARAP*)	× 2·4	NM_001307
Hypothetical protein LOC134466	× 2·3	AI242408
α-Tubulin-like	× 2·3	NM_145042
Human DNA sequence from clone RP5-1118D24 on chromosome 1p36.11–36·33	× 2·3	AL031276
Homo sapiens DNA-damage-regulated autophagy modulator 1 (*DRAM1*)	× 2·2	NM_018370
Annexin A2 (*ANXA2*) or lipocortin 2	× 2·1	M62895
Homo sapiens angiomotin-like 1 (*AMOTL1*)	× 2·1	NM_130847
Metallothionein-1X (*MT1X*)	× 1·8	NM_005952
Glutathione *S*-transferase pi 1 (*GSTP1*)	× 1·5	NM_000852
Down-regulated		
Myocardin-related transcription factor B (*MRTFB*)	× 0·26	AK093577
RAD9 homologue B (*RAD9B*)	× 0·29	AK058176
Clone IMAGE:4794726	× 0·36	BF513121
Hypothetical protein MGC34713	× 0·36	NM_173665
Small nuclear ribonucleoprotein polypeptide N	× 0·37	AU118874
Hypothetical gene supported by AK093253 (*LOC400579*)	× 0·38	BC033201
Cyclin-dependent kinase 6	× 0·59	AW192700
Homo sapiens ATG3 autophagy-related 3 homologue (*ATG3*)	× 0·59	NM_022488

British Journal of Nutrition

not answer why the expression of eNOS and SIRT1 was induced without involving PPAR due to the limitations of the present study.

Repeated treatments with resveratrol up-regulate the expression of autophagy-, radical scavenger activity- and anti-inflammatory activity-related genes and down-regulate the expression of a cell-cycle checkpoint control gene

To examine the expression of other differentially regulated genes following resveratrol treatment, DNA microarray analysis was performed. Using cut-off values of 1·5-fold for induction and 0·67-fold for suppression, 256 up-regulated and 411 down-regulated genes were identified. Among these candidate genes (Table 1), the up-regulation of the autophagy-related *GABARAP* gene[21] was confirmed by real-time quantitative RT-PCR (Fig. 2(a)). The induction of autophagocytosis by 50 μM-resveratrol and the extension of the autophagy-mediated lifespan have been reported previously[22,23]. In this context, we found that the expression of the autophagy-related *LC3B* and *AGT3* genes was also up-regulated by treatment with 1 μM-resveratrol for 6 d (Fig. 2(b) and (c)), although these were not detected in the microarray analysis. Autophagy plays key roles in adaptation to stress such as starvation and normal development of the immune system as well as in a wide range of disease states. Therefore, the beneficial effects of resveratrol could partly be explained by the up-regulation of the expression of autophagy-related genes (Fig. 2). On the other hand, the beneficial effects of fenofibrate on retinal pigment epithelium have recently been reported to be partly due to the induction of autophagy[24]; however, we could not observe the induction of the expression of autophagy-related genes by fenofibrate under our assay condition (data not shown).

The up-regulation of the expression of the radical scavenger activity-related *MT1X* (Fig. 3(a)) and anti-inflammatory activity-related annexin A2 (*ANXA2*; Fig. 3(b)) genes and the down-regulation of the expression the *RAD9B* gene (Fig. 3(c)) were also observed using real-time quantitative RT-PCR analysis. ANXA2 is reported to be a regulator of cell surface plasmin generation[25], and there are no reports on the function of RAD9B, but its gene is a homologue of *RAD9*, an evolutionarily conserved gene with multiple functions for preserving genomic integrity[26], indicating that the beneficial effects of resveratrol may partly be due to the up-regulation of the expression of the antioxidant *MT1X* and anti-inflammatory *ANXA2* genes and the down-regulation of the expression of the *RAD9B* gene. However, there were several discrepancies between the DNA microarray (Table 1) and real-time quantitative RT-PCR results for the angiomotin-like 1 (*AMOTL1*; Fig. 3(d)), *LOC134466* (Fig. 3(e)), glutathione *S*-transferase pi 1 (*GSTP1*; Fig. 3(f)), myocardin-related transcription factor B (*MRTFB*; Fig. 3(g)) and cyclin-dependent kinase 6 (*CDK6*; Fig. 3(h)) genes. Similarly, induction of the expression of the *eNOS* and *SIRT1* genes by resveratrol was detected using real-time quantitative RT-PCR (Fig. 1) but not by the microarray analysis. These results show that the DNA

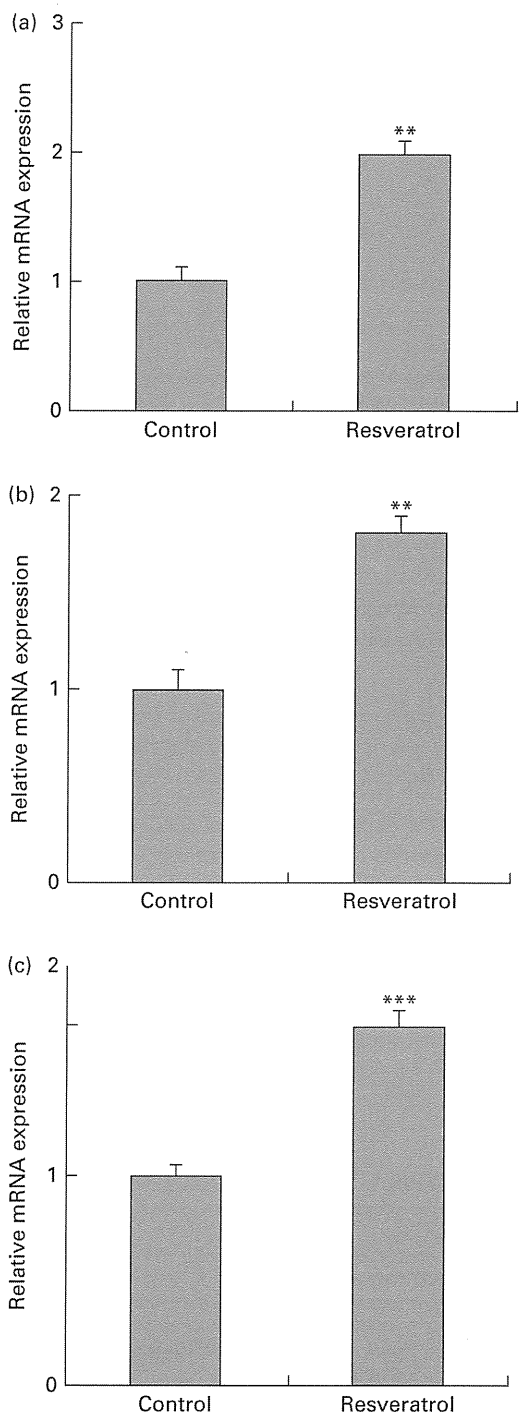

Fig. 2. Up-regulation of the expression of autophagy-related genes in human umbilical vein endothelial cells (HUVEC) following repeated treatments with 1 μM-resveratrol for 6 d. HUVEC were cultured in the presence or absence of 1 μM-resveratrol as described in Fig. 1, and isolated mRNA from the HUVEC was used for quantitative RT-PCR analysis. The level of each mRNA was normalised to that of the glyceraldehyde-3-phosphate dehydrogenase (*GAPDH*) mRNA. The normalised levels of the control mRNA are expressed as 1. The relative mRNA expression levels of (a) γ-aminobutyric acid A receptor-associated protein (*GABARAP*), (b) microtubule-associated protein 1 light chain 3B (*LC3B*) and (c) autophagy-related protein 3 (*ATG3*) are shown. Values are means of three separate dishes, with standard deviations represented by vertical bars. Mean values were significantly different from those of control: ** $P<0·01$ and *** $P<0·001$ (unpaired *t* test). Similar results were obtained by two additional experiments.

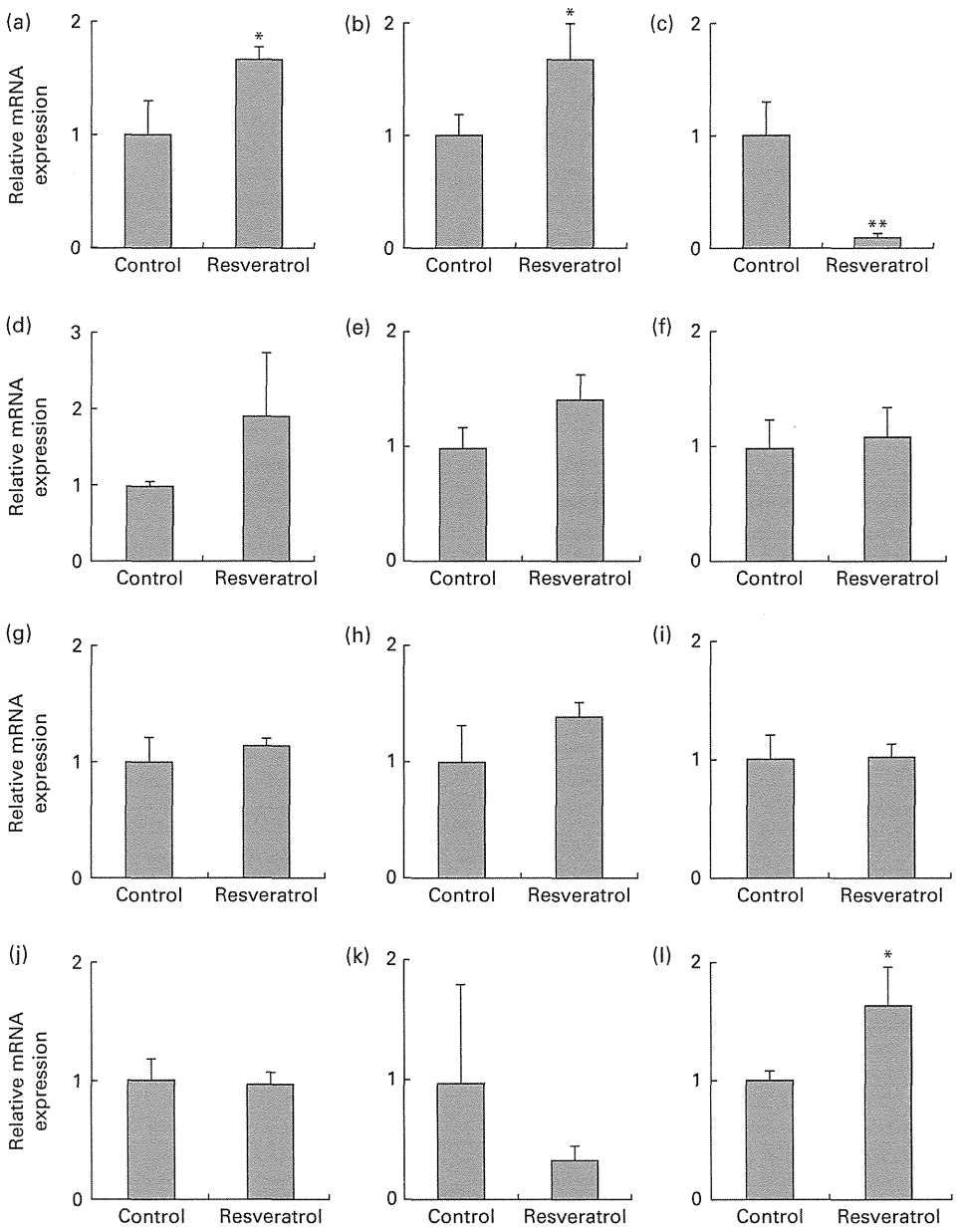

Fig. 3. Expression of the radical scavenger activity-, anti-inflammatory activity- and cell-cycle checkpoint control-related genes and cyclo-oxygenase 2 (*COX-2*), *PPARα*, *PPARβ/δ* and *PPARγ* genes in human umbilical vein endothelial cells (HUVEC) following repeated treatments with 1 μM-resveratrol for 6 d. The mRNA was isolated from the HUVEC for quantitative RT-PCR analysis following treatment with 1 μM-resveratrol for 6 d. The level of each mRNA was normalised to that of the glyceraldehyde-3-phosphate dehydrogenase (*GAPDH*) mRNA. The relative mRNA expression levels of (a) metallothionein-1X (*MT1X*), (b) anti-inflammatory activity-related annexin A2 (*ANXA2*), (c) RAD9 homologue B (*RAD9B*), (d) angiomotin-like 1 (*AMOTL1*), (e) *LOC134466*, (f) glutathione *S*-transferase pi 1 (*GSTP1*), (g) myocardin-related transcription factor B (*MRTFB*), (h) cyclin-dependent kinase 6 (*CDK6*), (i) *COX-2*, (j) *PPARα*, (k) *PPARβ/δ* and (l) *PPARγ* are shown. Values are means of three separate dishes, with standard deviations represented by vertical bars. Mean values were significantly different from those of control: * $P<0{\cdot}05$ and ** $P<0{\cdot}01$ (unpaired *t* test). Similar results were obtained by two additional experiments.

microarray analysis is useful for the screening of candidate genes, but this should be confirmed by real-time quantitative RT-PCR.

Finally, we examined the expression of COX-2 and PPAR. The expression of COX-2 was unchanged following resveratrol treatment (Fig. 3(i)). This is consistent with our previous observations that resveratrol suppresses the expression of COX-2 in 184B5/HER-transformed mammary epithelial cells[4], but not in BAEC (H Inoue, unpublished results), and that 15-deoxy-$\Delta^{12,14}$ PGJ_2, a natural PPARγ agonist, suppresses the expression of COX-2 in macrophage-like U937 cells, but not in BAEC[9]. The expression levels of PPARα (Fig. 3(j)) and PPARβ/δ (Fig. 3(k)) were also unchanged following resveratrol treatment; however, the expression of PPARγ was up-regulated (Fig. 3(l)). Increased expression of PPARγ had not been detected previously in BAEC[9], indicating possible differences between these cell lines.

In summary, we demonstrated that the expression of eNOS and SIRT1 is up-regulated in HUVEC following repeated treatments with a physiological concentration (1 μM) of

resveratrol for 6 d. These results will account, in part, for the cardiovascular benefits of the long-term consumption of red wine. Moreover, genes related to autophagy, radical scavenger activity, anti-inflammatory activity and cell-cycle checkpoint control were shown to be differentially regulated in this condition. Modulating the expression of these genes may contribute to the observed beneficial effects of resveratrol on the cardiovascular system.

Supplementary material

To view supplementary material for this article, please visit http://dx.doi.org/10.1017/S0007114513001670

Acknowledgements

We thank Dr Hiroko Shirotani-Ikejima, Dr Michiko Katsukawa, Ms Kumiko Satoh, Ms Chisako Ogura and Ms Naoko Anzai for their technical assistance. The present study was supported by a Grant-in-Aid for Scientific Research (no. 19300250 and 24300217 to H. I. and R. N.) from the Ministry of Education, Culture, Sports, Science and Technology of Japan, the Iijima Memorial Foundation for the Promotion of Food Science and Technology, and Japan Food Chemical Research Foundation. H. I., T. Y., R. Y. and R. N. designed the research. Y. T., Y. K., H. A., E. T. and A. T. performed the experiments and analysed the data. K. K. and T. M. coordinated the DNA microarray analysis. H. I., Y. T., Y. K. and R. N. discussed the results and wrote the manuscript. The authors declare that there are no conflicts of interest.

References

1. Lastra CA & Villegas I (2005) Resveratrol as an anti-inflammatory and anti-aging agent: mechanisms and clinical implications. *Mol Nutr Food Res* **49**, 405–430.
2. Baur JA & Sinclair DA (2005) Therapeutic potential of resveratrol: the *in vivo* evidence. *Nat Rev Drug Discov* **5**, 493–506.
3. Smith WL (2008) Nutritionally essential fatty acids and biologically indispensable cyclooxygenases. *Trends Biochem Sci* **33**, 27–33.
4. Subbaramaiah K, Chung WJ, Michaluart P, *et al.* (1998) Resveratrol inhibits cyclooxygenase-2 transcription and activity in phorbol ester-treated human mammary epithelial cells. *J Biol Chem* **273**, 21875–21882.
5. Inoue H, Jiang X, Katayama T, *et al.* (2003) Brain protection by resveratrol and fenofibrate against stroke requires peroxisome proliferator-activated receptor alpha in mice. *Neurosci Lett* **352**, 203–206.
6. Tsukamoto T, Nakata R, Tamura E, *et al.* (2010) Vaticanol C, a resveratrol tetramer, activates PPARα and PPARβ/γ *in vitro* and *in vivo*. *Nutri Metab* **7**, 46.
7. Michalik L, Auwerx J, Berger JP, *et al.* (2006) International Union of Pharmacology. LX1. Peroxisome proliferator-activated receptors. *Pharmacol Rev* **58**, 726–741.
8. Sonoda J, Pei L & Evans RM (2008) Nuclear receptors: decoding metabolic disease. *FEBS Lett* **9**, 2–9.
9. Inoue H, Tanabe T & Umesono K (2000) Feedback control of COX-2 expression through PPARγ. *J Biol Chem* **275**, 28028–28032.
10. Howitz KT, Bitterman KJ, Cohen HY, *et al.* (2003) Small molecule activators of sirtuins extend *Saccharomyces cerevisiae* lifespan. *Nature* **425**, 191–196.
11. Baur JA, Pearson KJ, Price NL, *et al.* (2006) Resveratrol improves health and survival of mice on a high-caloric diet. *Nature* **444**, 337–342.
12. Lagouge M, Argmann C, Gerhart-Hines Z, *et al.* (2006) Resveratrol improves mitochondrial function and protects against metabolic disease by activating SIRT1 and PGC-1α. *Cell* **127**, 1109–1122.
13. Kaeberlein M, McDonagh T, Heltweg B, *et al.* (2005) Substrate-specific activation of sirtuins by resveratrol. *J Biol Chem* **280**, 17038–17045.
14. Pacholec M, Bleasdale JE, Chrunyk B, *et al.* (2010) SRT1720, SRT2183, SRT1460, and resveratrol are not direct activators of SIRT1. *J Biol Chem* **285**, 8340–8351.
15. Wallerath T, Deckert G, Ternes T, *et al.* (2002) Resveratrol, a polyphenolic phytoalexin present in red wine, enhances expression and activity of endothelial nitric oxide synthase. *Circulation* **106**, 1652–1658.
16. Hotta M, Nakata R, Katsukawa M, *et al.* (2010) Carvacrol, a component of thyme oil, activates PPARα and γ, and suppresses COX-2 expression. *J Lipid Res* **51**, 132–139.
17. Inoue H, Taba Y, Miwa Y, *et al.* (2002) Transcriptional and posttranscriptional regulation of cyclooxygenase-2 expression by fluid shear stress in vascular endothelial cells. *Arterioscler Thromb Vasc Biol* **22**, 1415–1420.
18. Shirotani-Ikejima H, Kokame K, Hamuro T, *et al.* (2002) Tissue factor pathway inhibitor induces expression of *JUNB* and *GADD45B* mRNAs. *Biochem Biophys Res Commun* **299**, 847–852.
19. Takahashi S & Nakashima Y (2012) Repeated and long-term treatment with physiological concentration of resveratrol promotes NO production in vascular endothelial cells. *Br J Nutr* **107**, 774–780.
20. Hayashida S, Arimoto A, Kuramoto Y, *et al.* (2010) Fasting promotes the expression of SIRT1, an NAD^+-dependent protein deacetylase, via activation of PPARalpha in mice. *Mol Cell Biochem* **339**, 285–292.
21. Mohrlüder J, Schwarten M & Willbold D (2009) Structure and potential function of gamma-aminobutyrate type A receptor-associated protein. *FEBS J* **276**, 4989–5005.
22. Opipari AW Jr, Tan L, Boitano AE, *et al.* (2004) Resveratrol-induced autophagocytosis in ovarian cancer cells. *Cancer Res* **64**, 696–703.
23. Morselli E, Galluzzi L, Kepp O, *et al.* (2009) Autophagy mediates pharmacological lifespan extension by spermidine and resveratrol. *Aging* **1**, 961–970.
24. Miranda S, González-Rodríguez Á, García-Ramírez M, *et al.* (2012) Beneficial effects of fenofibrate in retinal pigment epithelium by the modulation of stress and survival signaling under diabetic conditions. *J Cell Physiol* **227**, 2352–2362.
25. Ling Q, Jacovina AT, Deora A, *et al.* (2004) Annexin II regulates fibrin homeostasis and neoangiogenesis *in vivo*. *J Clin Invest* **113**, 38–48.
26. Lieberman HB (2006) *Rad9*, an evolutionarily conserved gene with multiple functions for preserving genomic integrity. *J Cell Biochem* **97**, 690–697.

British Journal of Nutrition

Immunity
Article

The Satb1 Protein Directs Hematopoietic Stem Cell Differentiation toward Lymphoid Lineages

Yusuke Satoh,[1,7,8] Takafumi Yokota,[1,7,*] Takao Sudo,[1] Motonari Kondo,[2,9] Anne Lai,[2] Paul W. Kincade,[3] Taku Kouro,[4] Ryuji Iida,[3,4] Koichi Kokame,[5] Toshiyuki Miyata,[5] Yoko Habuchi,[1] Keiko Matsui,[1] Hirokazu Tanaka,[1,10] Itaru Matsumura,[1,10] Kenji Oritani,[1] Terumi Kohwi-Shigematsu,[6] and Yuzuru Kanakura[1]

[1]Department of Hematology and Oncology, Osaka University Graduate School of Medicine, Suita, Osaka 565-0871, Japan
[2]Department of Immunology, Duke University Medical Center, Durham, NC 27710, USA
[3]Immunobiology and Cancer Program, Oklahoma Medical Research Foundation, Oklahoma City, OK 73104, USA
[4]Laboratory of Immune Modulation, National Institute of Biomedical Innovation, Ibaraki, Osaka 567-0085, Japan
[5]Department of Molecular Pathogenesis, National Cerebral and Cardiovascular Center, Suita, Osaka 565-8565, Japan
[6]Department of Cell and Molecular Biology, Lawrence Berkeley Laboratory, University of California, Berkeley, Berkeley, CA 94720, USA
[7]These authors contributed equally to this work
[8]Present address: Department of Lifestyle Studies, Kobe Shoin Women's University, Kobe 657-0015, Japan
[9]Present address: Department of Immunology, Toho University School of Medicine, Tokyo 143-8540, Japan
[10]Present address: Division of Hematology, Department of Internal Medicine, Kinki University School of Medicine, Osaka 589-8511, Japan
*Correspondence: yokotat@bldon.med.osaka-u.ac.jp
http://dx.doi.org/10.1016/j.immuni.2013.05.014

SUMMARY

How hematopoietic stem cells (HSCs) produce particular lineages is insufficiently understood. We searched for key factors that direct HSC to lymphopoiesis. Comparing gene expression profiles for HSCs and early lymphoid progenitors revealed that Satb1, a global chromatin regulator, was markedly induced with lymphoid lineage specification. HSCs from Satb1-deficient mice were defective in lymphopoietic activity in culture and failed to reconstitute T lymphopoiesis in wild-type recipients. Furthermore, Satb1 transduction of HSCs and embryonic stem cells robustly promoted their differentiation toward lymphocytes. Whereas genes that encode Ikaros, E2A, and Notch1 were unaffected, many genes involved in lineage decisions were regulated by Satb1. Satb1 expression was reduced in aged HSCs with compromised lymphopoietic potential, but forced Satb1 expression partly restored that potential. Thus, Satb1 governs the initiating process central to the replenishing of lymphoid lineages. Such activity in lymphoid cell generation may be of clinical importance and useful to overcome immunosenescence.

INTRODUCTION

To maintain the immune system, hematopoietic stem cells (HSCs) differentiate to lymphoid-primed multipotent progenitors (LMPPs) and then to lymphoid-specified progenitors in a process accompanied by the loss of erythroid-megakaryocyte and myeloid potential (Adolfsson et al., 2005; Lai and Kondo, 2008). Accumulating evidence has suggested that combinations of transcription factors coordinately and sequentially regulate lymphopoiesis. Five transcription factors, PU.1, Ikaros, E2A, EBF, and Pax5 are hierarchically involved in the early steps of B-lineage differentiation (Medina et al., 2004). Whereas EBF and Pax5 specifically act in B-lineage-determined progenitors, PU.1 and Ikaros are expressed in earlier hematopoietic progenitors and involved in multiple lineage decision processes (Scott et al., 1997; Yoshida et al., 2006). E2A, an indispensable factor for B lymphopoiesis, can also affect T lymphocyte formation by regulating Notch1 expression (Ikawa et al., 2006). Furthermore, recent reports have shown that E2A proteins are expressed in primitive hematopoietic progenitors and play a critical role in early lymphoid specification (Dias et al., 2008; Yang et al., 2008; Semerad et al., 2009). However, whether the initiation of lymphoid differentiation is regulated entirely by transcription factors in a hierarchical manner remains unclear.

The immune system changes qualitatively and quantitatively with ontogeny and age (Miller and Allman, 2005; Montecino-Rodriguez and Dorshkind, 2006). Indeed, lymphocyte progenitors expand substantially in the fetal liver (FL), but their production shifts to bone marrow (BM) and becomes stable after birth. With age, replenishment of the adaptive immune system declines (Rossi et al., 2005; Sudo et al., 2000). Qualitative changes in lymphopoietic activity of HSCs are reflected in in vitro cell-culture experiments. If key inducers in early lymphoid lineages can be identified, they will be useful for expanding lymphocytes in culture for clinical purposes. Additionally, manipulating the expression of relevant genes might boost the immune system of immunocompromised and elderly people.

We have developed a method to sort early lymphoid progenitors (ELPs) from Rag1-GFP reporter mice (Igarashi et al., 2002; Yokota et al., 2003a). ELPs expressing Rag1 are present in the $Sca1^{+}c\text{-}kit^{hi}$ HSC-enriched fraction; they displayed high B and T lymphopoietic potential, but limited myeloerythroid potential and self-renewal ability. In contrast, $Rag1^{-}Sca1^{+}c\text{-}kit^{hi}$ HSCs effectively reconstitute and sustain the lymphohematopoietic system for long periods in lethally irradiated recipients. We conducted gene array comparisons between those two fractions

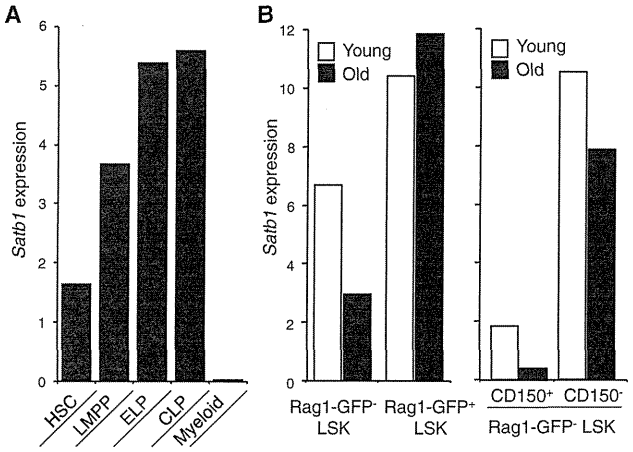

Figure 1. *Satb1* Expression Levels Change with Differentiation and Aging of HSCs

HSCs, LMPP, ELP, CLP, and the myeloid progenitor-enriched fractions were sorted from BM of 8- to 10-week-old Rag1-GFP knockin or WT mice according to cell surface markers and GFP expression (see Experimental Procedures), and transcripts for *Satb1* were quantitatively evaluated with real-time RT-PCR. (B) The LSK Rag1-GFP$^-$ and LSK Rag1-GFP$^+$ fractions (left panel) or the CD150$^+$ LSK Rag1-GFP$^-$ and CD150$^-$ LSK Rag1-GFP$^-$ fractions (right panel) were sorted from 6-week-old or 2-year-old Rag1-GFP knockin mice, respectively. Then *Satb1* expression was evaluated with real-time RT-PCR. The *Satb1* expression values were normalized by *Gapdh* expression and shown in each panel. Each data represents two independent examinations that showed essentially the same results (Figure 1; see also Figure S1 and Table S1).

with the goal of discovering molecules involved in the transition of HSCs to lymphoid lineages.

Herein, we showed that special AT-rich sequence binding 1 (Satb1), a nuclear architectural protein that organizes chromatin structure, plays an important role in lymphoid lineage specification. In parallel with or ahead of key transcription factors, the expression of Satb1 increased with early lymphoid differentiation. In functional assays, lymphopoietic activity was compromised in Satb1-deficient hematopoietic cells, but the induced expression of Satb1 strongly enhanced lymphocyte production from HSCs. Furthermore, exogenous Satb1 expression primed lymphoid potential even in embryonic stem cell (ESC)-derived mesoderm cells and aged BM-derived HSCs. Global analysis of potential Satb1 target genes identified a number that may have critical roles in early lymphopoiesis. The findings demonstrate that the earliest steps in lymphopoiesis are regulated by an epigenetic modifier and indicate how modulation of the process might be used to induce or rejuvenate the immune system.

RESULTS

Profiling Gene Expression of Rag1$^+$ ELP in Fetal Liver

We sorted the Rag1^{lo} c-kit^{hi} Sca1$^+$ ELP fraction and the Rag1$^-$ c-kit^{hi} Sca1$^+$ HSC-enriched fraction with high purity from E14.5 FL of Rag1-GFP knockin heterozygous embryos and performed gene arrays. We found that transcripts of *Trbv14* and *Ighm* genes were upregulated even in very early lymphoid progenitors (see Table S1 available online). Furthermore, we detected increased expression of *Il7r*, *Notch1*, and *Flt3* genes encoding cell surface receptors important for B or T lymphocyte differentiation in the ELP fraction. In addition to discovering many signal transduction kinases with unknown functions in lymphopoiesis, our search identified *Lck* and *Xlr4b* genes as being involved in lymphoid differentiation signals. Transcripts for some of these lymphoid-related genes had already been detected in the Rag1$^-$ HSC-enriched fraction (see the microarray data; accession number CBX73). These results suggest that lymphoid-lineage specification begins even before the emergence of Rag1^{lo} ELP. Additionally, the microarray data identified new candidate genes that might be important for early lymphoid development.

Expression of *Satb1* Increases with Early Lymphoid Specification and Declines with Age

Our major goal was to find key genes involved in the specification of lymphoid fates. Because the microarray data showed that expression of various lymphoid-related genes was activated before the ELP stage, we hypothesized the existence of a modulator that synchronously regulates multiple genes. Among the list in Table S1, *Satb1* attracted attention because it was originally identified as a protein binding to the enhancer region of the *Igh* gene and later shown to play a critical role in T cell development (Alvarez et al., 2000; Dickinson et al., 1992). Additionally, recent studies had demonstrated that it serves as a master regulator for many genes, including cytokines, cytokine receptors, and transcription factors (Cai et al., 2006; Han et al., 2008; Notani et al., 2010; Yasui et al., 2002).

To explore possible relationships between Satb1 and early lymphopoiesis, we examined its expression in primitive hematopoietic progenitors. The HSC-enriched Rag1-GFP$^-$ Flt3$^-$ lineage marker-negative (Lin$^-$) Sca1$^+$ c-kit^{hi} (LSK) fraction, the LMPP-enriched fraction, the ELP-enriched fraction, the common lymphoid progenitor (CLP)-enriched fraction, and the myeloid progenitor-enriched Lin$^-$ c-kit^{hi} Sca1$^-$ fraction were sorted from BM of 8- to 10-week-old mice. Transcripts for *Satb1* were then quantitatively evaluated with real-time RT-PCR. *Satb1* expression increased substantially when HSC differentiated into LMPP and ELP (Figure 1A). This trend matched that of other early lymphoid lineage-related genes including those that encode PU.1 (*Sfpi1*), Ikaros (*Ikzf1*), E2A (*Tcf3*), and Notch1 (Figure S1). Importantly, in contrast to its expression in the lymphoid lineage, *Satb1* expression was shut off when HSC differentiated to committed myeloid progenitors. These results suggest that *Satb1* is potentially involved in early lymphoid differentiation.

Lymphopoietic activity becomes compromised during aging. Accumulating evidence suggests that the earliest lymphoid progenitor pools proximal to HSC are deficient in aged BM (reviewed by Miller and Allman, 2005). Indeed, the Rag1$^+$ ELP population markedly decreases with age (data not shown). The downregulation of genes mediating lymphoid specification and function is likely a major cause (Rossi et al., 2005). Because *Satb1* has been listed in microarray panels as a downregulated gene in aged HSC (Chambers et al., 2007; Rossi et al., 2005), we sorted Rag1-GFP$^-$ LSK and ELP-enriched Rag1-GFP$^+$ LSK from BM of 6-week-old or 2-year-old Rag1-GFP heterozygous mice and examined their expression. In agreement with previous studies, our real-time RT-PCR identified an approximate 50% reduction of *Satb1* transcripts in aged Rag1-GFP$^-$ LSK cells (Figure 1B, left panel). The few ELP recovered from aged mice

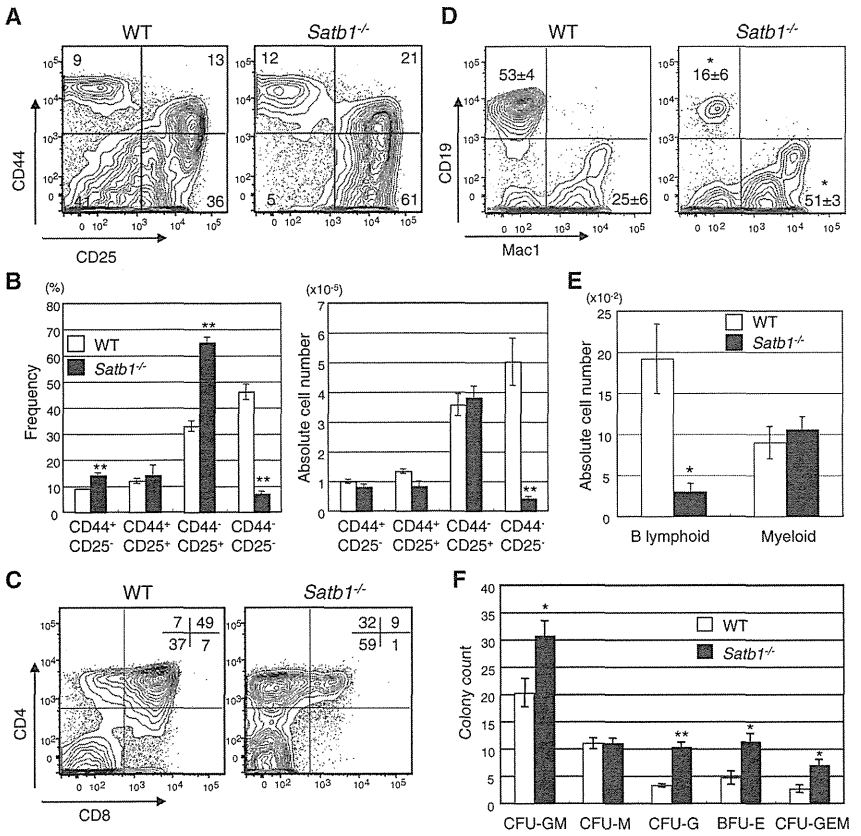

Figure 2. Satb1 Deficiency Alters Lymphoid and Myeloid Activities of Hematopoietic Stem/Progenitor Cells in Culture

Lin$^-$ cells were isolated from FL of E14.5 *Satb1*$^{-/-}$ embryos or their WT littermates.

(A–C) Cells were cocultured with OP9-DL1 stromal cells for evaluation of T-lineage differentiation. (A) Flow cytometry results are shown for cells recovered on day 14 and stained for CD44 and CD25/IL-2Rα. (B) Frequencies and absolute numbers of each phenotype were calculated. (C) A similar analysis was performed for CD4 and CD8α bearing cells recovered cells on day 18.

(D and E) The same cell suspensions were cocultured with MS5 stromal cells to assess B and myeloid lineage potentials and representative data are shown for day 7 of culture.

(F) In parallel, the Lin$^-$ cells were evaluated with methylcellulose colony assays. Each dish contained 1,000 sorted cells and colony counts were performed on day 10. The bars indicate numbers of CFU-GM, CFU-M, CFU-G, BFU-E, or CFU-GEM scored per dish. The results are shown as mean ± SE. Statistically significant differences between WT and *Satb1*$^{-/-}$ cells are marked with asterisks (*$p < 0.05$, **$p < 0.01$) (Figure 2; see also Figure S2).

expressed amounts of *Satb1* comparable to those in ELP from young mice. Recent purification methods for HSC with CD150, a SLAM family receptor that marks HSC even in aged BM (Yilmaz et al., 2006), identified an approximate 80% reduction in *Satb1* transcripts in aged HSC compared with ones from young mice (Figure 1B, right panel). These observations suggest that *Satb1* may be a key molecule related to immunosenescence.

Satb1 Deficiency Reduces the Lymphopoietic Activity of Hematopoietic Stem and Progenitor Cells

T cell development in the thymus is impaired in *Satb1*$^{-/-}$ mice (Alvarez et al., 2000). Although the profile of B220, immunoglobulin M (IgM), and IgD expression appears to be unaffected in the *Satb1*$^{-/-}$ spleen, the total number of B cells is reportedly reduced to approximately 25% of wild-type (WT) at 2 weeks of age (Alvarez et al., 2000). We have determined that the number and frequency of cells that can be recovered from lymphoid organs were reduced in E18.5–19.5 *Satb1*$^{-/-}$ fetuses. Body sizes of *Satb1*$^{-/-}$ fetuses were not different from WT and heterozygous littermates (Figures S2A and S2B).

We then sorted Lin$^-$ cells from FL of *Satb1*$^{-/-}$ mice or their WT littermates and cultured them with stromal cells that support lymphopoiesis. T cell differentiation can be recapitulated in vitro with hematopoietic cells cultured with OP9 expressing the Notch ligand Delta-like 1 (OP9-DL1). Under these coculture conditions, the differentiation patterns of WT and *Satb1*$^{-/-}$ Lin$^-$ cells differed significantly (Figures 2A and 2B). The majority of *Satb1*$^{-/-}$ cells were arrested in the CD44$^-$CD25$^+$ stage and did not differentiate into CD44$^-$CD25$^-$ cells. Reduction of IL-7 from culture media normally induces maturation of the CD4$^-$CD8$^-$ double-negative (DN) into CD4$^+$CD8$^+$ double-positive (DP) cells and subsequently into either the CD4$^+$ or the CD8$^+$ single-positive cells. However, more than half of the *Satb1*$^{-/-}$ cells were arrested in DN stages even after the IL-7 reduction, and their differentiation to the DP stage was aberrantly skewed toward CD4$^+$CD8$^-$ (Figure 2C).

Substantial differences were also observed in B-lineage cell production. In coculture with MS5, which supports B and myeloid lineages in the presence of SCF, Flt3-ligand, and IL-7, *Satb1*$^{-/-}$ progenitors exhibited significant reductions in B-lymphopoietic potential (Figures 2D and 2E). Coculture with OP9, which originated with M-CSF-deficient mice and supported the B lineage predominantly, also yielded reduced B/myeloid ratios with *Satb1*$^{-/-}$ progenitors (Figure S2C). Essentially the same results were obtained when cultures were initiated with LSK Flt3$^-$, more stringently purified HSC (Figure S2D, 2E). In addition, B cell lineage output was also reduced when *Satb1*$^{-/-}$ LMPP or CLP were cultured (Figure S2F). In contrast, the myeloid potential was retained in *Satb1*$^{-/-}$ progenitors (Figures 2D and 2E). Indeed, the Lin$^-$ fraction of E14.5 *Satb1*$^{-/-}$ FL contained more myeloid-erythroid progenitors than that of the WT control (Figure 2F).

In transplantation experiments, we observed that CD45.2$^+$ *Satb1*$^{-/-}$ HSC sorted from 2-week-old BM did not effectively reconstitute CD3$^+$ T-lineage cells in lethally irradiated CD45.1$^+$ WT recipients (Figure 3A). Peripheral blood CD3$^+$ T-lineage recoveries from *Satb1*$^{-/-}$ HSC were decreased approximately 90% compared with that from WT HSC (Figure 3B). Conversely, we observed varied amounts of reconstitution of the B lineage and no reduction in reconstitution of the myeloid lineage

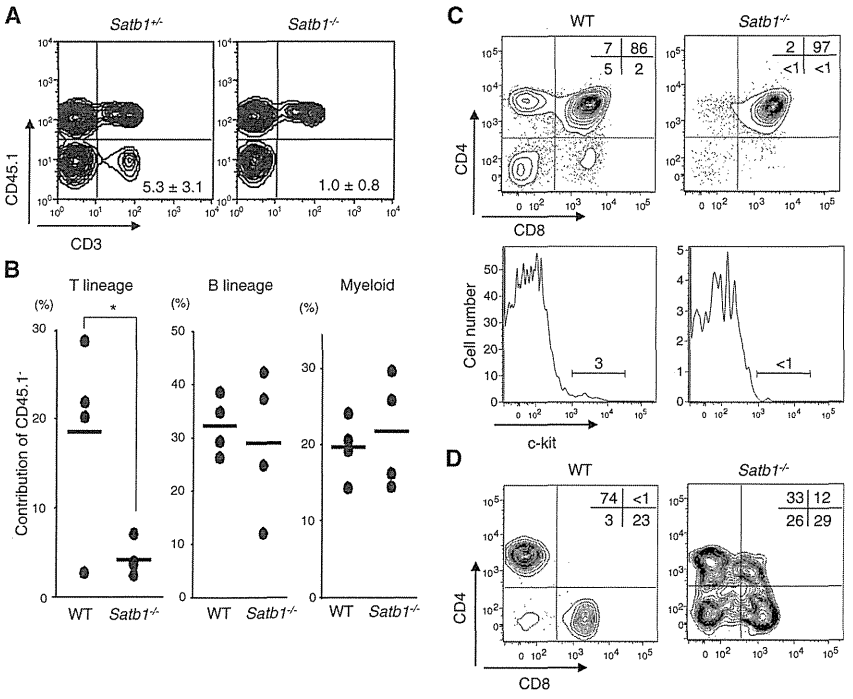

Figure 3. Defective T Lymphopoiesis from Transplanted *Satb1*$^{-/-}$ HSC

(A and B) One thousand stem-cell-enriched Flt3$^-$ LSK cells were sorted from BM of 2-week-old Satb1 deficient or littermate mice (CD45.2). They were then mixed with 4 × 10^5 adult BM cells obtained from WT (CD45.1) mice and were transplanted into lethally irradiated WT CD45.1 mice. At 8 weeks after transplantation, peripheral blood cells of the recipients were identified with anti-CD45.1 and anti-CD3. Numbers in each panel of (A) represent percentages of CD3$^+$ CD45.1$^-$ cells among the total leukocytes and are shown as averages with SD (n = 4 in each). Chimerisms of CD45.1$^-$ cells in the CD3$^+$ T-lineage, the CD45R/B220$^+$ B lineage, or the Gr1$^+$ myeloid lineage were determined. Statistical significance is *p < 0.05. (C and D) One thousand Flt3$^-$ LSK cells sorted from E14.5 FL of Satb1 homodeficient or their WT littermates (CD45.2) were transplanted into lethally irradiated WT CD45.1 mice. At 8 weeks after transplantation, T-lineage reconstitution in the thymus and the spleen was analyzed. The CD4 and CD8 profiles of CD45.2$^+$ thymocytes (C, upper panels) and the c-kit expression of CD45.2$^+$ CD3$^-$ CD4$^-$ CD8$^-$ CD44$^+$ CD25$^-$ thymocytes (C; lower panels) are shown. (D) Representative CD4 and CD8 profiles are shown for CD45.2$^+$ CD3$^+$ cells in recipient spleens.

resulted from Satb1 ablation (Figure 3B). Compromised T cell lineage contributions of *Satb1*$^{-/-}$ HSC were also evident in the thymus and spleen (Figures 3C and 3D). Although T lymphopoiesis in the thymus was replaced by either WT or *Satb1*$^{-/-}$ donor cells when FL HSCs were transplanted, thymocytes were reduced in the *Satb1*$^{-/-}$ recipients and their differentiation was affected. Besides apparent stagnation at the DP stage and marked reduction of the DN population (Figure 3C, upper panels), c-kit^{hi} cells in the CD44$^+$CD25$^-$ DN1 stage were rare in *Satb1*$^{-/-}$ recipients (Figure 3C, lower panels). The reduced contribution of *Satb1*$^{-/-}$ cells was also evident in CD3$^+$ splenic T lymphocytes. Interestingly, T cells in the spleens of *Satb1*$^{-/-}$ recipients contained substantial percentages of DP and DN cells. Such T cell lineage cells are extremely rare in normal mouse spleens (Figure 3D).

Taken together, these results demonstrate that Satb1 is indispensable for normal T lymphopoiesis, but not for myelopoiesis. The factor may normally have a lesser role in B-lineage differentiation. Furthermore, our data indicate that abnormalities of lymphoid development observed in *Satb1*$^{-/-}$ mice are intrinsic to *Satb1*$^{-/-}$ hematopoietic cells.

Forced Expression of Satb1 in HSC Induces Lymphopoiesis

Next we conducted overexpression experiments to define the role of Satb1 in lineage-fate decisions of HSCs. LSK Flt3$^-$ cells were sorted from BM of adult WT mice and then retrovirally transduced with either a fluorescence-alone expressing control or a native Satb1 construct combined with a GFP-expressing vector. Successfully transduced cells were sorted according to GFP expression. Real-time RT-PCR and immunoblots revealed that Satb1-transduced cells expressed more than 10-fold *Satb1* transcripts and Satb1 proteins compared to control cells (Figure S3A).

The sorted cells were cultured with stromal cells that supported lymphopoieisis. Results from these experiments complemented the observations with *Satb1*$^{-/-}$ cells. Satb1 transduction enhanced T cell lineage growth in OP9-DL1 cocultures (Figures 4A and 4B). By day 10 of the culture, cells had been increased more than 5-fold by Satb1-transduction, and a majority of the recovered cells had progressed to the DN2 and DN3 stages. Differentiation to the DP stage was also advanced by the Satb1-transduction (Figure 4A). The kinetics of cell differentiation and expansion in the B cell lineage showed more changes. Whereas both control and Satb1-transduced cells produced substantial numbers of B-lineage cells, the latter produced B220$^+$CD19$^+$ cells more quickly and efficiently (Figure S3B). Specifically, the Satb1 transduction resulted in approximately 50- to 300-fold and 5-fold greater recovery of B220$^+$CD19$^+$ cells on day 10 in the MS5 and OP9 cocultures, respectively (Figures 4C and 4D). Notably, Satb1 transduction negatively influenced the output of myeloid cells, particularly Mac1^{lo}Gr1$^+$ granulocytes (Figure S3C). In addition, CFU-GM formation of HSC was decreased by Satb1 transduction (Figure S3D).

In stromal-free cultures containing SCF, Flt3-ligand, and IL-7, Satb1 expression strongly induced CD19$^+$ cell production from the LSK fraction (Figure S3E). When calculated on a per-cell basis, one LSK cell with Satb1 overexpression produced approximately 450 CD19$^+$ cells, whereas only 50 cells with this B-lineage marker were produced from control progenitors. As for other hematopoietic lineages, DX5$^+$CD3e$^-$ NK cells emerged when IL-15 was added to the stromal cell-free cultures. Coexpression of NK1.1 and/or CD94 confirmed the NK-lineage, and

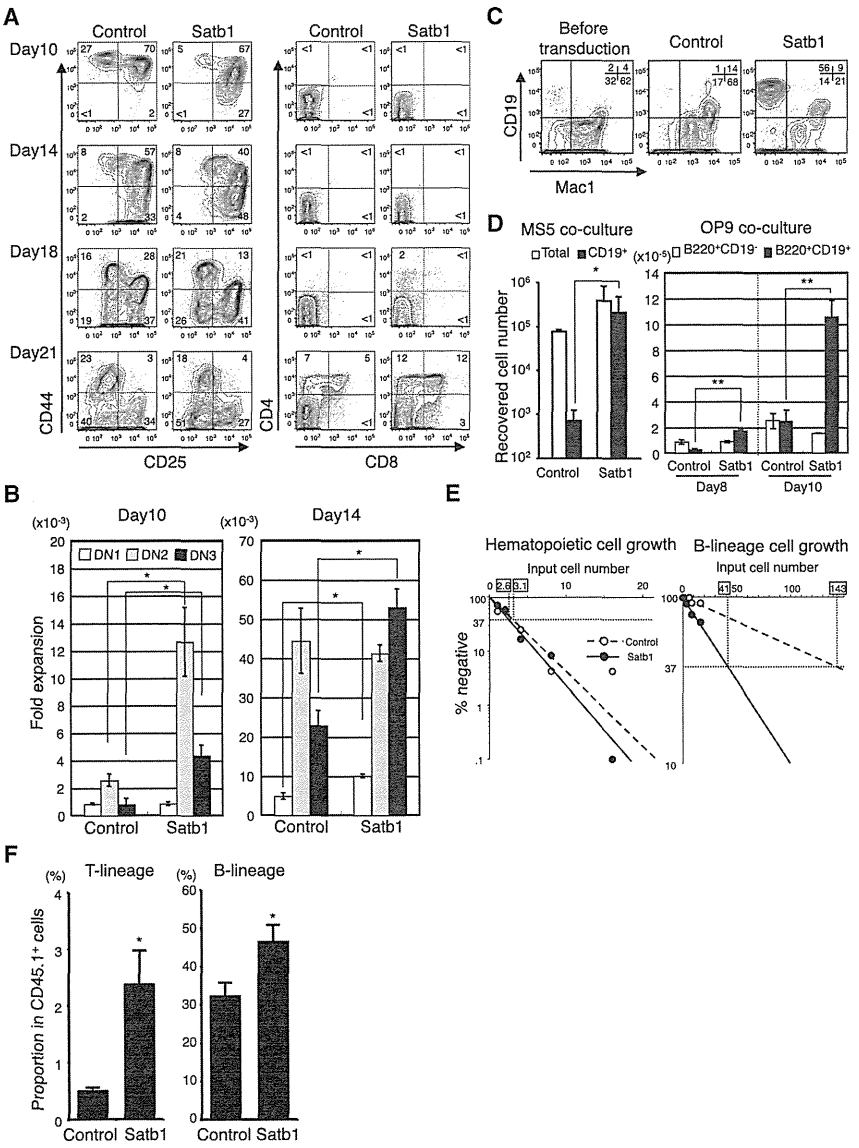

Figure 4. Satb1 Overexpression Promotes Lymphopoiesis

LSK Flt3$^-$ cells obtained from WT BM were retrovirally transduced with either a fluorescence-alone expressing control or a native Satb1 combined with GFP expressing vector. Successfully transduced cells were cultured, and their differentiation and proliferation were analyzed at the indicated period.

(A and B) Time-course analyses were performed for T-lineage cell generation in the OP9-DL1 coculture. Absolute numbers of recovered cells were divided by the numbers of transduced LSK Flt3$^-$ cells used to initiate the cultures to obtain the fold expansion values. Data are shown as mean ± SE.

(C) CD19 and Mac1 profiles are shown for cells recovered from MS5 cocultures on day 10. The left panel shows data obtained from fresh LSK Flt3$^-$ cells that did not undergo the retroviral infection.

(D) The absolute numbers of total recovered cells and B-lymphoid cells in the MS5 coculture (left panel). The output of B220$^+$ CD19$^-$ or B220$^+$ CD19$^+$ B-lineage cells was evaluated in the OP9 coculture (right panel). Cultures were established in triplicate. Data are shown as mean ± SE. Statistical significance is *$p < 0.05$, **$p < 0.01$.

(E) Limiting-dilution analyses were performed to determine the frequencies of hematopoietic progenitors that could give rise to CD19$^+$ B-lineage cells. Input cell numbers corresponding to each 37% negative value are shown in rectangles.

(F) One thousand LSK Flt3$^-$ cells (CD45.1) transduced with either Satb1-expressing or control vectors were transplanted to lethally irradiated WT mice (CD45.2) with 1 × 10^5 adult BM cells (CD45.2). Two weeks after transplantation, peripheral blood was collected to determine the proportion of CD4/CD8$^+$ T lineage and CD19$^+$ B lineage in CD45.1$^+$ cells. Data are shown as mean ± SE. Statistical significance is *$p < 0.05$. ($n = 5$ in each group) (Figure 4, see also Figure S3).

their numbers were also enhanced by Satb1 overexpression (Figure S3F). Interestingly, the same Satb1-transduced LSKs differentiated to neither conventional nor plasmacytoid dendritic cells (Figure S3G).

The results from in vitro bulk cultures and assessment of lymphoid lineage cell numbers might reflect enhanced survival of lymphoid progenitors rather than priming or expansion of lymphoid potential in individual clones. Notably, no obvious increase in apoptotic cells occurred in any tested cultures with *Satb1*$^{-/-}$ cells or *Satb1*$^{-/-}$ lymphopoietic organs (data not shown and Figure S3H). Additionally, Satb1 overexpression conferred growth advantages to hematopoietic progenitors without influencing their viability in any of the cultures we used (data not shown). To investigate further the mechanisms through which Satb1 exerts its effect on early progenitors, we performed limiting dilution assays. On average, 1 in 3.1 control cells and 1 in 2.6 Satb1-transduced cells gave rise to blood cells, indicating that both are highly potent progenitors for hematopoietic cell growth (Figure 4E, left). Nevertheless, we observed significant differences between them regarding the frequencies of progenitors with lymphopoietic potential. While 1 in 41 Satb1-transduced Flt3$^-$ LSK cells produced B cells, only 1 in 143 control cells were lymphopoietic under these conditions (Figure 4E, right). In the same experiment, fresh Flt3$^-$ LSK cells without retroviral transfection produced hematopoietic cells and B cells at a frequency of 1 in 6.7 cells and 1 in 61 cells, respectively (data not shown).

These results suggest that Satb1 expression affects early lineage decisions in individual HSC and expands the growth and differentiation of lymphoid cells in vitro. To evaluate whether these findings were of practical value, we performed in vivo transplantation experiments with SATB1-transduced LSK Flt3$^-$ cells. We observed enhanced contribution of the SATB1-transduced cells to both T and B lineages in short-term engraftment (Figure 4F). To assess whether the overexpression of SATB1 induces tumors, we evaluated long-term and short-term

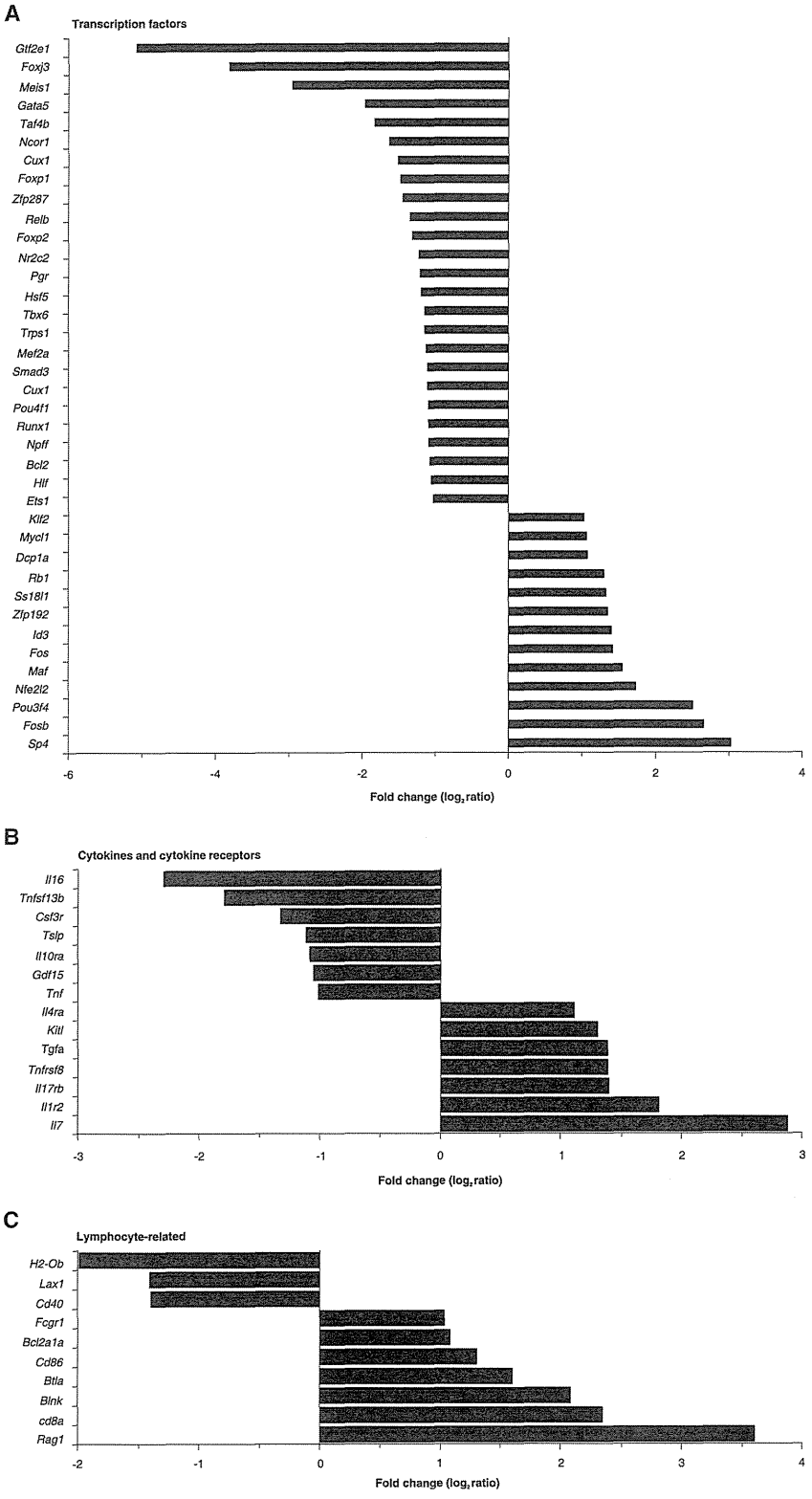

Figure 5. Genes Affected by Satb1 Expression

A microarray experiment was performed to compare gene expression in Satb1 and control-transduced LSK Flt3$^-$ cells. Upregulation in Satb1-transduced cells is shown as positive in each figure. (A) Transcription factors, (B) cytokine and cytokine receptors, and (C) other lymphoid lineage-related genes are summarized (Figure 5; see also Tables S2 and S3).

Satb1 Regulates Lymphoid Lineage-Related Genes in HSC

During early lymphocyte differentiation, several transcription factors have been shown to play roles in a hierarchical manner. To identify the target genes of Satb1, we first examined whether the exogenous expression of Satb1 influences the expression of lineage-relevant transcription factors in LSK Flt3$^-$ cells. Although high Satb1 expression was achieved, no significant upregulation was observed in the expression of *Sfpi1*, *Ikzf1*, *Tcf3*, or *Notch1* (data not shown). The expression of *Cebpa*, which is important for myeloid differentiation, was also not significantly affected (data not shown).

Next, to find candidate genes involved in the Satb1 induction of lymphopoiesis, we performed a microarray comparing gene expression between Satb1- and control-transduced LSK Flt3$^-$ cells (Table S2). In accordance with the results described above, the data showed no significant changes in the expression of *Sfpi1*, *Ikzf1*, *Tcf3*, *Notch1*, or *Cebpa*. However, several transcription factors involved in lymphoid differentiation, *Sp4*, *Maf*, *Fos*, and *Id3*, were upregulated in Satb1-transduced cells (Figure 5A). Cytokines such as *Il7* and *Kitl*, which are critical for lymphocyte differentiation and generally believed to be stromal cell products, were induced in hematopoietic progenitor cells themselves by ectopic expression of Satb1 (Figure 5B). While receptors for IL-4 or IL-17 were induced, *Csf3r*, encoding the G-CSF receptor, was downregulated. Interestingly, among lymphoid-related genes, *Rag1*, which is indispensable for both T and B cell differentiation, was strongly induced by Satb1 (Figure 5C). Expression of the CD86 gene that correlates with lymphoid competency (Shimazu et al., 2012) was also significantly elevated.

lymphohematopoiesis after transplantation. In eight transplanted mice, SATB1-overexpressing cells did not induce tumors, at least during 3 months of observation.

As a complementary experiment, we performed a set of microarray analyses comparing gene expression signatures between WT and *Satb1*$^{-/-}$ cells (Table S3). We again observed no direct correlations between Satb1 expression and *Ikzf1*, *Tcf3*, or *Notch1*, but confirmed that the expression of numerous lineage-related genes was influenced. The expression of *Il7* and *Kitl* was detectable in WT hematopoietic progenitors, and their levels were significantly lower in the *Satb1*$^{-/-}$ progenitors. Of note, *Satb2*, which is a homolog of *Satb1*, as well as *Bright*, which codes a B cell-specific AT-rich sequence binding protein (Herrscher et al., 1995), were upregulated in *Satb1*$^{-/-}$ HSC. In addition, the *Satb1*$^{-/-}$ HSC aberrantly expressed *Rag1* and *Pax5*, whose levels decreased with differentiation to LMPP. These results indicate that Satb1 expression globally influences many genes involved in lineage-fate decisions during the specification of HSC toward lymphoid lineages.

Satb1 Induces Lymphopoiesis in ESCs

Next, we examined whether the exogenous expression of Satb1 is sufficient to promote lymphopoiesis in ESCs. In the OP9 coculture system (Nakano et al., 1994), ESCs can produce mesoderm cells in 4.5 days, which have potential to become hematopoietic and endothelial cells. After a short period of retroviral transduction with the control-GFP or the Satb1-GFP vector, ES-derived mesoderm cells were cultured with OP9 in the presence of SCF, Flt3-ligand, and IL-7. As shown in Figure 6A, although both control- and Satb1-transfected cells contained substantial numbers of GFP$^+$ cells, the latter produced CD45$^+$ hematopoietic cells efficiently. Further phenotype revealed that most of the CD45$^+$ GFP$^+$ cells produced from the Satb1-transfected cells expressed B220 and CD19 (Figure 6A, right panels). Notably, those cells were also positive for AA4.1, CD11b, and CD5, suggesting that they were likely B1-B-lineage cells (Figure 6B).

Next, we established ESC clones, which can be induced to express Satb1-GFP on removal of tetracycline (Tet) from the culture medium. Eight days after Tet deprivation (day 12.5; Figure 6C), approximately 15% of the recovered cells were GFP$^+$ (data not shown). Thirty-five percent of these cells expressed CD45 and included substantial numbers of AA4.1$^+$ CD19$^+$ B-lineage cells (Figure 6D, right panels). Conversely, in the presence of Tet, the proportions of AA4.1$^+$ and CD19$^+$ cells among the CD45$^+$ faction were very low (Figure 6D, left panels). A majority of the CD19$^+$ cells among the Satb1-GFP$^+$ ES-derived cells were positive for Mac1 or CD5, again indicating a preference for the B1-B lineage (Figure 6E). In cytospin preparations, many of the ES-derived cells cultured with Tet showed myelomonocytic morphology, whereas Satb1/GFP$^+$ cells exhibited lymphocyte-like morphology (Figure 6F). Finally, a PCR-based *Igh* rearrangement assay confirmed D_H-J_H recombination in the Satb1-GFP$^+$ ES-derived cells (Figure 6G).

To test T-lineage potential, we transduced the control-GFP or the Satb1-GFP vector to ES-derived mesoderm cells and cultured them with OP9-DL1 cells. The Satb1-transduced cells effectively produced CD4$^+$ CD8$^+$ DP cells with rapid kinetics (Figures 6H and 6I). Substantial numbers of ES-derived T-lineage cells expressed TCR-γδ or TCR-β, and Satb1-transduced cells were advanced in this regard (data not shown). Taking these results together, we conclude that Satb1 expression directs even ES-derived cells toward lymphoid lineages.

Ectopic Satb1 Expression in Aged HSC Restores Lymphopoietic Potency

As shown in Figure 1B, the *Satb1* expression in HSC declines with age. This decline might be correlated with the age-dependent impairment of lymphopoiesis. Therefore, we examined whether Satb1 expression restores the lymphopoietic activity of progenitors from aged mice. Rag1-GFP$^-$ LSK cells of 2-year-old mice were transduced with control or Satb1-DsRed vectors. After 72 hr of transduction, DsRed$^+$ cells were sorted and cultured on OP9 in the presence of SCF, Flt3-ligand, and IL-7. The Satb1-transduced cells produced a percentage of Rag1-GFP$^+$ B220$^+$ cells that was significantly higher than that of control cells (Figure 7A). Indeed, most of the aged Rag1-GFP$^-$ LSK cells were prone to differentiate into Rag1-GFP$^+$ cells as a result of exogenous Satb1 expression. With respect to the recovered B-lineage cell counts, approximately 3-fold more B220$^+$ Rag1-GFP$^+$ Mac1$^-$ cells were obtained through Satb1 overexpression (Figure 7B).

Conversely, fewer B-lineage cells were generated from aged ELP than from young ELP despite their similar expression of *Satb1* (Figure 1B; Figure S4A). B-lineage differentiation of aged ELP also showed decreased Rag1 expression (Figure S4B). Nonetheless, aged ELP showed substantial lymphopoietic activity in MS5 cocultures, in which aged HSC scarcely produced B-lineage cells (Figure S4A). These results suggest that the downregulation of Satb1 expression is involved in the compromised lymphopoietic potential of aged HSC and that ectopic induction of Satb1 can at least partially restore the activity.

DISCUSSION

Despite accumulating evidence that multiple transcription factors support lymphocyte differentiation, ones that specifically direct HSC to the lymphoid lineage have remained elusive. One aim of this study was to describe molecular signatures of early stages of lymphopoiesis by comparing gene expression patterns between HSC and ELP. While we observed that many genes specific for the lymphoid lineage including *Tcr*, *Igh* and *Il7r* were highly induced at the ELP stage, some lymphoid genes were already expressed at low levels in the HSC-enriched fraction. Among them, we were particularly interested in chromatin modifiers because of their ability to control spatial and temporal expression of essential genes. Our screen identified Satb1, whose expression was previously linked to T lymphocyte differentiation (Alvarez et al., 2000). We show that Satb1 plays a critical role in directing HSC to lymphoid lineages.

Satb1 was originally identified as a protein that binds specifically to genomic DNA in a specialized DNA context with high base-unpairing potential (termed base-unpairing regions; BURs) (Dickinson et al., 1992). Satb1 is predominantly expressed in the thymus and subsequent studies revealed critical roles in thymocyte development (Alvarez et al., 2000), T cell activation (Cai et al., 2006), and Th2 differentiation (Notani et al., 2010). In thymocyte nuclei, Satb1 has a cage-like distribution and tethers BURs onto its regulatory network, thus organizing 3-dimensional chromatin architecture (Cai et al., 2003). By recruiting chromatin modifying and remodeling factors, Satb1 establishes region-specific epigenetic status at its target gene loci and regulates a large number of genes (Yasui et al., 2002;

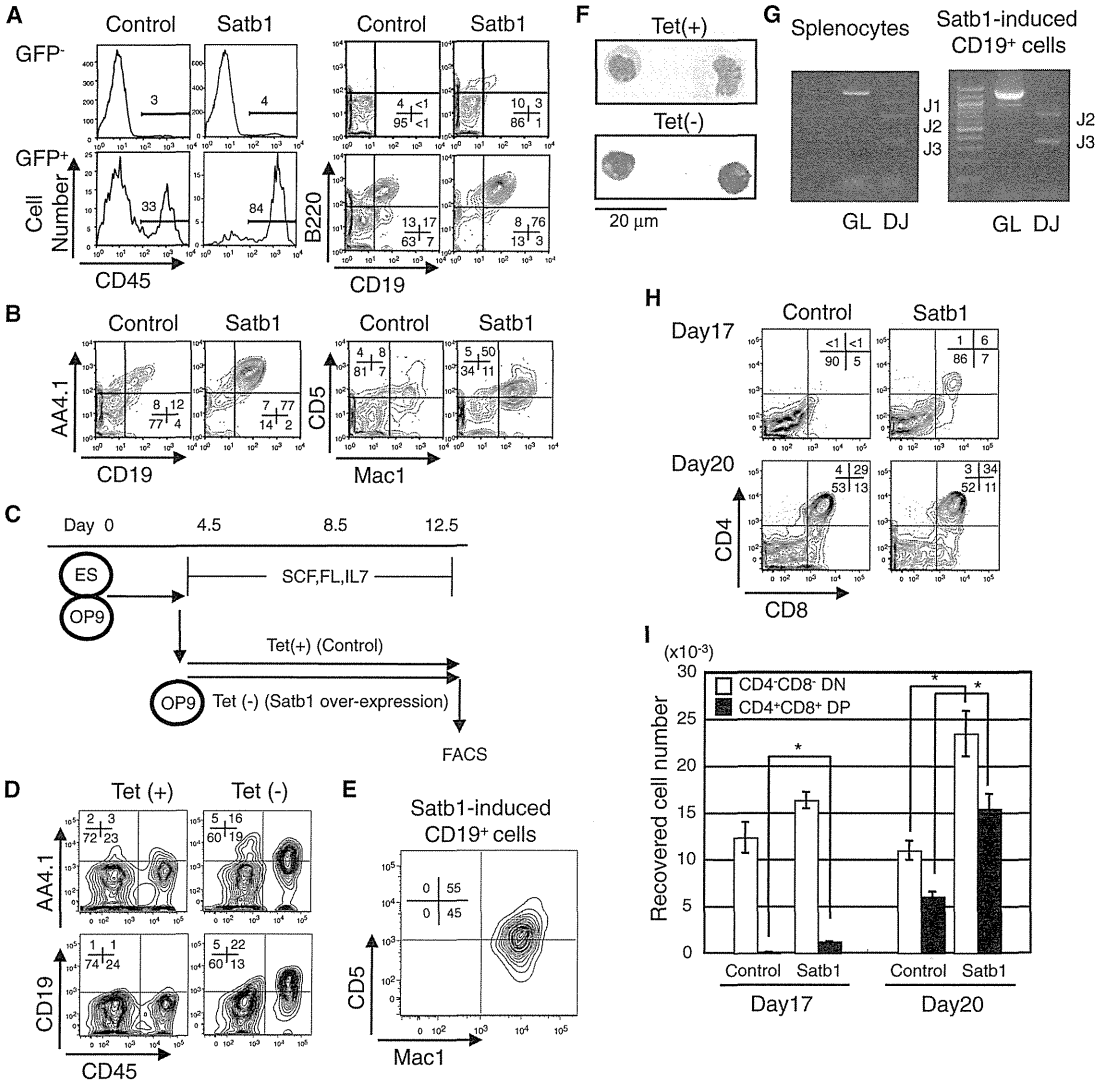

Figure 6. Satb1 Promotes Lymphoid Differentiation from ES-Derived Cells

E14tg2a ESCs were deprived of leukemia inhibitory factor and seeded onto OP9 cells. After 4.5 days, the differentiated mesoderm cells were infected with retroviral supernatants containing control-GFP or Satb1-GFP expressing vectors. Subsequently, the cells were cultured on OP9 for 8 days. At the end of culture, all cells were harvested and stained with the antibodies indicated in each panel.

(A) Total recovered cells were divided according to GFP expression (left panels). The percentages of $CD45^+$ cells in GFP^- (upper panels) and GFP^+ populations (lower panels) are shown. CD45R/B220 and CD19 profiles of the $CD45^+$ cells corresponding to the left panels (right panels) are shown.

(B) Representative AA4.1 and CD19 or Mac1 and CD5 profiles of the GFP^+ $CD45^+$ cells recovered from control or Satb1-transduced culture.

(C) The experimental design used with a Tet-off system (upper panel). ESCs, which inducibly express Satb1 by Tet deprivation, were established. After 4.5 days of culture without leukemia inhibitory factor in the presence of Tet, the differentiated cells were reseeded onto new OP9 stromal cells with or without Tet. Subsequently, FACS analysis was performed after 8 days of culture (day 12.5).

(D) Tet (+) indicates profiles of GFP^- cells cultured with Tet (left panels). Tet (–) panels show profiles of Satb1/GFP^+ cells cultured without Tet (right panels).

(E) Mac1 and CD5 expression on the Satb1/GFP^+ $CD19^+$ cells grown without Tet.

(F) Morphology of ES-derived hematopoietic cells on day 12.5.

(G) DNA PCR assays of germline (GL) or D_H-J_H rearranged *Igh* chain (DJ) genes were performed with the Satb1/GFP^+ $CD19^+$ cells recovered without Tet (right panel). Splenocytes were used as a positive control for the D_H-J_H recombination (left panel). On each gel, a size marker was loaded in the left lane.

(H and I) E14tg2a ESCs were differentiated to mesoderm cells for 4.5 days and then infected with the retroviral supernatant containing control-GFP or Satb1-GFP expressing vectors for 3 days. Subsequently, the cells were cultured on OP9-DL1 and T-lineage output was evaluated on the indicated days. Data are shown as mean ± SE. Statistical significance is $*p < 0.05$.

Cai et al., 2003). Increased Satb1 expression in hematopoietic progenitors compared with HSC has been observed by others (Forsberg et al., 2005; Ng et al., 2009); however, no study has been conducted concerning the role of Satb1 in differentiation of HSC to either lymphoid or myeloid progenitors. Our results clearly show a tight association of Satb1 expression with